IN THIS ISSUE

London Journals Press

IMAGE: OBSERVATORY WITH STAR TRAILS ON MOUNTAINS FOR CLEAR SKY

www.journalspress.com

LONDON JOURNAL OF RESEARCH IN SCIENCE: NATURAL AND FORMAL

Print ISSN: 2631-8490
Online ISSN: 2631-8504
DOI: 10.17472/LJRS

Volume 23 | Issue 1 | Compilation 1.0

COMPILED IN UNITED KINGDOM

ENGLISH

London Journal of Research in Science: Natural and Formal

Volume 23 | Issue 3 | Compilation 1.0

PUBLISHER

London Journals Press
1210th, Waterside Dr, Opposite Arlington Building, Theale, Reading
Phone:+444 0118 965 4033 Pin: RG7-4TY United Kingdom

SUBSCRIPTION

Frequency: Quarterly

Print subscription
$280USD for 1 year
$500USD for 2 year
(color copies including taxes and international shipping with TSA approved)

Find more details at https://journalspress.com/journals/subscription

ENVIRONMENT

London Journals Press is intended about protecting the environment. This journal is printed using led free environmental friendly ink and acid-free papers that are 100% recyclable.

London Journals Press Headquaters

1210th, Waterside Dr,
Opposite Arlington
Building, Theale, Reading
Phone:+444 0118 965 4033
Pin: RG7-4TY
United Kingdom

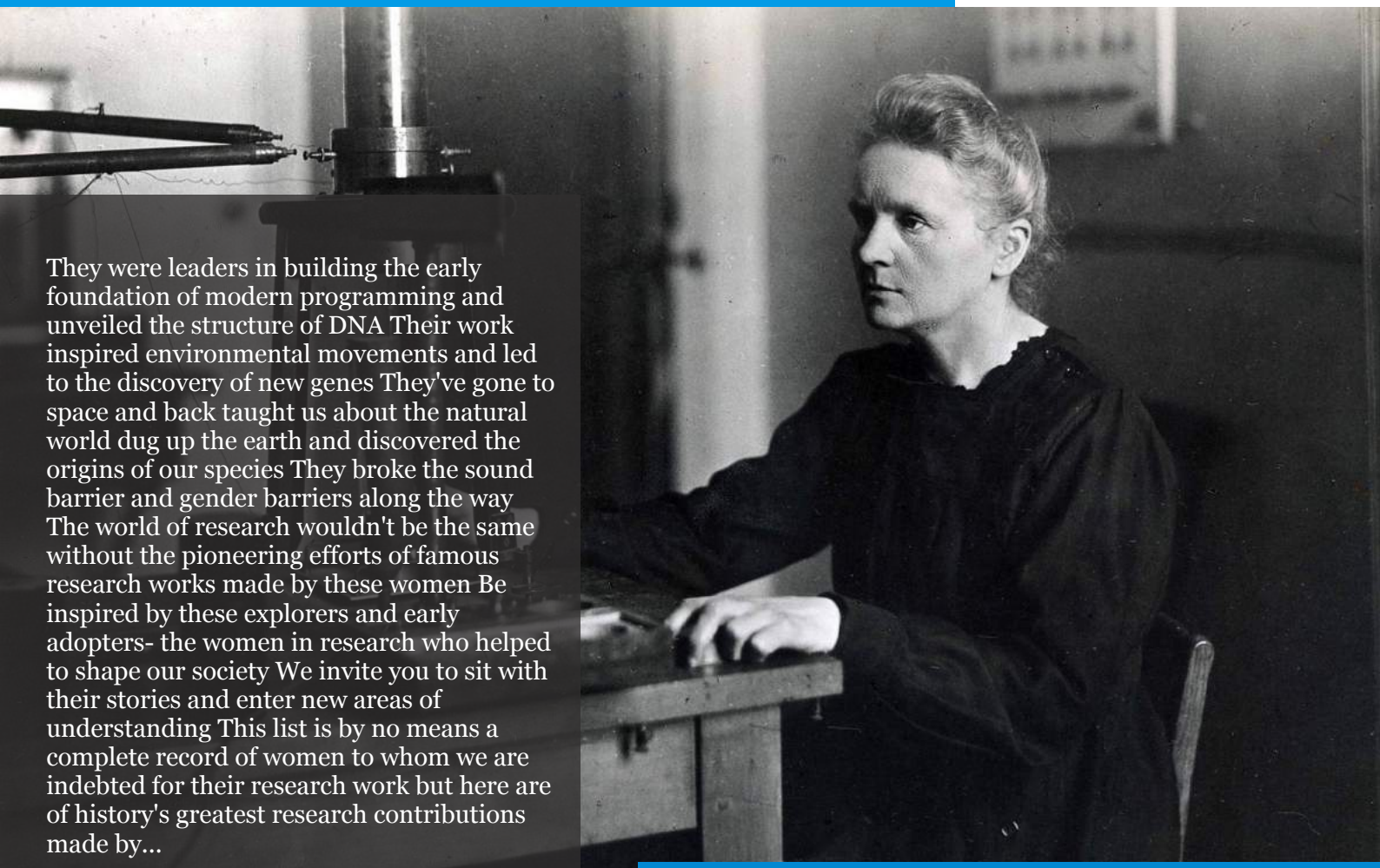

They were leaders in building the early foundation of modern programming and unveiled the structure of DNA Their work inspired environmental movements and led to the discovery of new genes They've gone to space and back taught us about the natural world dug up the earth and discovered the origins of our species They broke the sound barrier and gender barriers along the way The world of research wouldn't be the same without the pioneering efforts of famous research works made by these women Be inspired by these explorers and early adopters- the women in research who helped to shape our society We invite you to sit with their stories and enter new areas of understanding This list is by no means a complete record of women to whom we are indebted for their research work but here are of history's greatest research contributions made by...

Read complete here:
https://goo.gl/1vQ3lS

Women In Research

Computing in the cloud!

Cloud Computing is computing as a Service and not just as a Product Under Cloud Computing...

Read complete here:
https://goo.gl/VvHC72

Writing great research...

Prepare yourself before you start Before you start writing your paper or you start reading other...

Read complete here:
https://goo.gl/np73jP

Journal Content
In this Issue

London Journals Press

Editorial Board

Curated board members

Nicola Mastronardi

Consiglio Nazionaledelle Ricerche,
Ph.D. Applied Mathematics Katholieke
Universiteit Leuven
Belgium

Dr. Indranil Sen Gupta

Ph.D., Mathematics
Texas A & M University
Department of Mathematics
North Dakota State University
North Dakota, USA

Dr. Arvind Chhabra

University of Connecticut Health Center
USA Ph.D., Biotechnology Central
Drug Research Institute

Dr. Vladimir Burtman

Research Scientist
The University of Utah
Geophysics
Frederick Albert Sutton Building
115 S 1460 E Room 383
Salt Lake City, UT 84112, US

Dr. Xianghong Qi

University of Tennessee
Oak Ridge National Laboratory
Center for Molecular Biophysics
Oak Ridge National Laboratory
Knoxville, TN 37922
United States

Dr. Arshak Poghossian

Ph.D. Solid-State Physics
Leningrad Electrotechnical Institute, Russia
Institute of Nano and Biotechnologies
Aachen University of Applied Sciences, Germany

Dr. Bingyun Li

Ph.D. Fellow, IAES
Guest Researcher, NIOSH, CDC, Morgantown, WV
Institute of Nano and Biotechnologies
West Virginia University, US

Dr. Maria Gullo

Ph.D., Food Science, and Technology
University of Catania
Department of Agricultural and Food Sciences
University of Modena and Reggio Emilia, Italy

Dr. A. Heidari

Ph.D., D.Sc
Faculty of Chemistry
California South University (CSU), United States

Dr. Alicia Esther Ares

Ph.D. in Science and Technology,
University of General San Martin, Argentina
State University of Misiones, US

Research papers and articles

Volume 23 | Issue 3 | Compilation 1.0

The Crematory Key to the Greenhouse Effect with Volcanic Ashes: The Key of the Anthropocene Resides in Human Cremation. The Dangerous Loop that Remains to be Smashed to End Global Warming Definitively

Florent Pirot

ABSTRACT

In the word anthropocene lays the implicit of the cannibalism and its explanation rests actually on the crematory activities which can be shown to be acutely related to it, so much that it seems that the wording was invented by "ditching" researchers attempting to whistleblow without exposing themselves to too much exclusion costs in a society overall supportive of it. Global warming spills from volcanic tephras establishing the greenhouse under which human emissions of heat cause the climate heat-up but crematory ashes falling into subduction trenches make volcanic tephras thicker and laws of kinetics bringing progressively everything down make the ashes everyday closer to the trenches. While most winds are the result of crematory activities and of their particular antigravitons (except for old mass burial sites near magmatic areas), they also accelerate the above pattern of descent into trenches and create a dangerous loop which can be demonstrated in other ways.

Keywords: NA

Classification: DDC Code: 179.1 LCC Code: QC981.8.G56

Language: English

London Journals Press

LJP Copyright ID: 925621
Print ISSN: 2631-8490
Online ISSN: 2631-8504

London Journal of Research in Science: Natural and Formal

Volume 23 | Issue 3 | Compilation 1.0

The Crematory Key to the Greenhouse Effect with Volcanic Ashes: The Key of the Anthropocene Resides in Human Cremation. The Dangerous Loop that Remains to be Smashed to End Global Warming Definitively

Florent Pirot

ABSTRACT

In the word anthropocene lays the implicit of the cannibalism and its explanation rests actually on the crematory activities which can be shown to be acutely related to it, so much that it seems that the wording was invented by "ditching" researchers attempting to whistleblow without exposing themselves to too much exclusion costs in a society overall supportive of it. Global warming spills from volcanic tephras establishing the greenhouse under which human emissions of heat cause the climate heat-up but crematory ashes falling into subduction trenches make volcanic tephras thicker and laws of kinetics bringing progressively everything down make the ashes everyday closer to the trenches. While most winds are the result of crematory activities and of their particular antigravitons (except for old mass burial sites near magmatic areas), they also accelerate the above pattern of descent into trenches and create a dangerous loop which can be demonstrated in other ways. The heat-up needed for crematory activities itself contributes to global warming and there is a latent pollution from alpha emitters resulting to the fission deficit that causes more long-term rises, compelling to announce a coming disaster if drastic measures are not taken.

I. INTRODUCTION

The eruption of the Raikoke in June 2019 has been an interesting opportunity to observe the effects of crematory dumps in the deep sea trenches on volcanism. There is a clear effect of Soviet submarines around, and of tokamak-mash weapons from the end of the 1970s also dumped in, in the resulting tephra plume.

London Journal of Research in Science: Natural and Formal

Figure 1: NASA Earth Observatory, June 22th 2019

Crematory ovens have been used in Delta-3 class Soviet submarines (for instance) for the upward kick to break the ice, with also the loss of mass converted into energy for theoretically perfect icebreak[1], with certainly a downward throw of the crematory matter for maximal "Archimedes push" icebreak. The USSR also used frequently crematory power in siloing pattern with tunnel retchlags and nitrogen injection on the victims getting out of the uranium tunnel mine just to stumble immediately into the tunnel, where nitrogen was injected before neutron work, for the making of primitive ICBMs with a crematory nuclear propulsion[2]. Crematory systems were also common in Gorbachev-era artillery and there is also an effect of the Earth's spin and flow of crematory sludge from the Alaska (both civilian and military activities) and of the alpha emitters in the oil of the Exxon Valdez oil spill altogether.

[1] Causing ulterior loss of control of the return into the water, facilitating surprise identification of the submarine stranded on the ice by enemy powers. Especially as nuclear reactor handlers were the most likely to be incinerated for the needs of the rise since they were usually the most contaminated.

[2] This has been also used by the Chinese communist regime more recently against Uighurs.

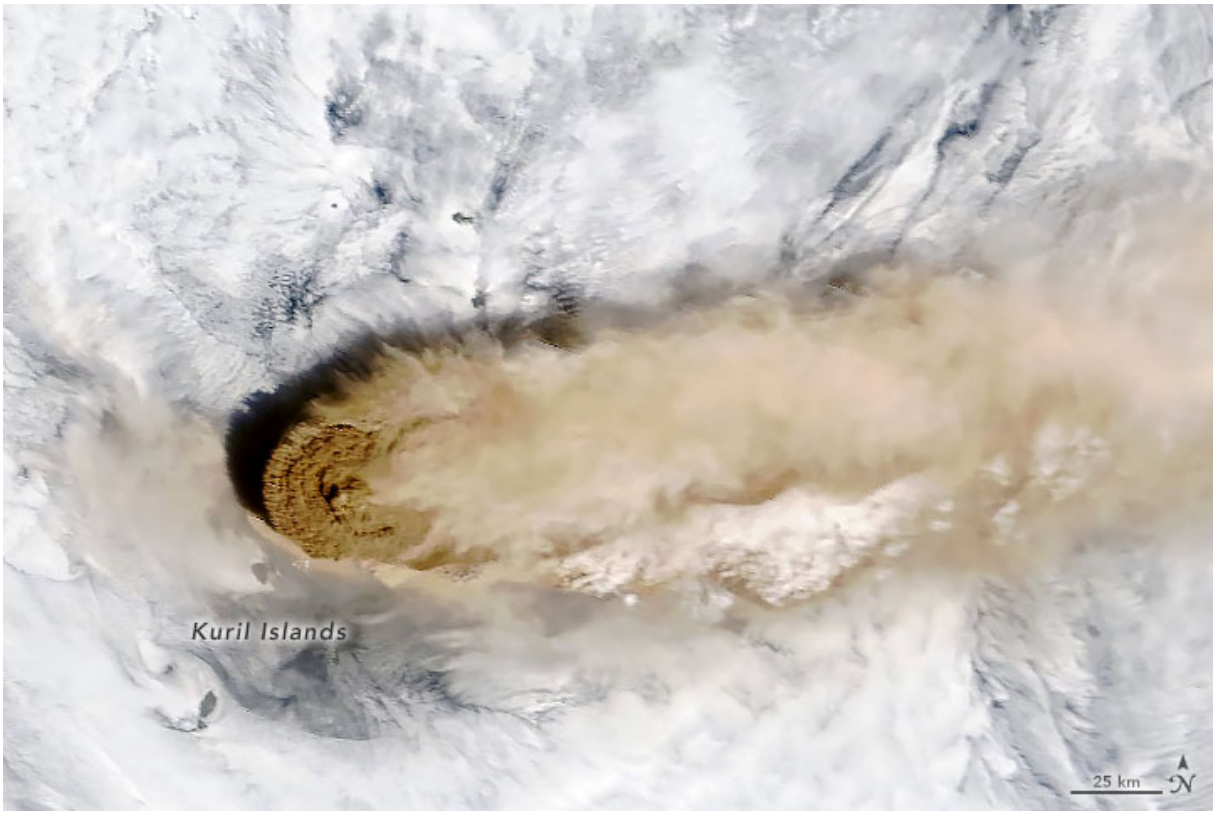

Figure 2: NASA picture, 22th of June 2019, the tokmash (tokamak-mash) component is here particularly visible

The study of the 20th Century list of major volcanic eruptions shows that there is a more global pattern related to the dumping of crematory matter into lakes, rivers and sea trenches, after local discovery of the relative inefficiency versus clean nuclear fuels. It is clear by observing a picture of the local area of the Cerro Azul that it was the site of the first dumping of crematory ashes, after understanding of the weakness by the engineers of the Spanish Armed Forces who later followed in the Spanish Civil War Francisco Franco. This is followed, the year after, by the Bezymianny eruption, which clearly explains the later massive purges within the Red Army by Joseph Stalin, and his refusal to give to support the opponents to Francisco Franco in Spain.

The St Helens eruption in 1980 has clearly been boosted by a local understanding of the weakness of crematory oven ashes, perhaps in the China Lake military base, and subsequent river dumping. It is followed 2 years after by harmonization in Mexico explaining the intensity of the El Chichon eruption. The story of the Pinatubo 1991 eruption is clearly and definitively related to immediate pre-war efforts against Communist China following the quasi fall of the USSR, with the project of a nuclear reactor build onto the sleeping volcano, in particular, for supporting these future war efforts, explaining in particular the volcanic eruption – the light grey colour of the tephra column of the Pinatubo does not show significant levels of crematory contamination. The Eyjafjallajokull eruption however has to be linked to the economic crisis of Iceland starting from 2008, and elimination of crematory power cars after fall of demand (in relation to the earlier "bank overproduction" – in a small island-country in particular banking can be expected to be related to the basic model of the "banker seating on the stock of gold and silver", but in this case pressurizing a crematory system, so the economic crisis leads to excess "anthropic" [1] nuclear stocks).

These results, when brought together with intensity of outside use of crematory weapons, explain perfectly the essential of the global land and ocean temperature anomalies of the NOAA on the 20th Century. There is a visible effect of the massive use of crematory oven shells during WW2 until 1944, the end of rafles and the liberation of the extermination camps allows the downfall of temperatures

from 1945. There is a subsequent effect, certainly, of the transfer of the crematory technology in the civilian sector, where the limited heat-up related to the non-inflammability of most human corpses is frequently used for "cold" energy, together with a high disease risk, that has to be considered as the founder of the 1945-1976 consensus with a flat temperature curve and a strong public healthcare system to compensate.

This "coldness" of crematory energy is a lying concept as demonstrated by the subsequent climate effects of the volcanic tephras released when subduction has taken in the crematory ashes. The crematory ashes create a particularly thick veil that is the true "greenhouse effect" (already described in [2]) and the description above allows to show how the crematory component is a particularly strong trigger of subsequent global warming under tephras carrying it. The crematory component is a last-call result of a pattern itself immediately costly for the climate, since cremation demands heating and immediately (or through energy costs related for setting up of the particular infrastructure) that heating is released in the environment as well, causing more warming. One example at the beginning of the Ukraine War allowed to show that, with a large series of BTR-80s of the Ukrainian Army destroyed by Russian strikes ; a few days after temperatures fell down and snow came back on the Alps, allowing to ski again (in spite of a contamination with crematory plutonium following)[3].

A third element has to be taken into account as well, related to the low levels of fission in a crematory weapon. Although it may seem protective of the warming levels in a statistical computation related to *immediate* heat release, in a bomb format the heat release is intrinsically related to military efficiency, and low fission levels mean perdition in nature of most of the alpha emitters in addition to military defeat – since it is a result of the low transmutation (plutogenization) levels in the crematory phase. Their later alpha decay will contribute to support global warming, especially as solar neutrons progressively transmutate them and then fission them, meaning simply on the very long term a delayed and much less energy-efficient "delivery of the energy" whose characteristics are that it contributes much more to climate change and much less to the military purpose theoretically adjudicated. This is a result of the decision to do two things with a simple tool (the bomb), i.e. social / ethnic purge (by adopting the crematory, or mash, production system) and military strike altogether, causing long-term impossibility (cf. Lipsey-Lancaster paradox – the Avro-Manchester was a Western example of plane with a crematory propulsion, losses during WW2 testify of the neutron efficiency statistics theorems already at the basis of the first article written on the subject [3], with 63% of losses, in relation to the 33% usual yield of crematory oven power versus clean power, augmented by solar neutrons. More than 97% of cancers were estimed to be related to alpha emitters in [4]. The remaining can be associated to UVs [5] and solar neutrons. The crematory rate of plutogenization in the Avro Manchesters was obviously augmented by solar neutrons and also by UVs because they spinned the shuriken atoms frequently laterally (because of dawn raids) favorizing neutron capture, explaining entirely the survival rate of these planes. The Lipsey-Lancaster paradox demonstrates the imperative to not think of civilian or military nuclear power with other aims also in aims to definitively escape long-term failure).

All of these factors come together to explain climate curves in a definitive and imperative way. Human action has to be dragooned in a way prohibiting definitively all crematory activities and most mash activities as well (except when correctly inserted within human rights). *Pyroprocessing* in particular denominates the heat-up of nuclear systems in ways accelerating artificially neutron transfer, certainly associated to plutogenization of human ashes resulting in explosions particularly dense in climate-warming materials, through direct plumes of the explosions or through later volcanic redistribution. Following on earlier results of the author communicated early to health authorities regarding crematory and mash and diseases (more recently published in [6]), the Bulletin of the Atomic Scientists recently attempted to make the argument against crematory methods in a silent way by condemning pyroprocessing and strongly discouraging the regarding of plutonium as long term source of pollution at the same time [7], implicitly recognizing somehow the value of clean plutonium weapons. The article also points to the Argonne Laboratory's May 2001 claim to an energy policy review group led by Vice-President Dick Cheney of the development of a "proliferation-resistant"

[3] The mobile crematory format demands heating in a way that cannot be shielded, except at the cost of mobility of the tank. BTR-80s use reactor incineration and in this regard emit particularly high amounts of heat during the crematory plutogenization process (above called simply crematory process).

pyroprocessing retreatment of spent fuel, which certainly incited to the later use of depleted uranium weapons in developing countries while it is likely the result of a misunderstanding with woodfire heat-up of depleted uranium into argon in a cistern without any anthropic component actually developed in Argonne. Hydrogen can be used for pyroprocessing as well as all types of woods but banning "pyroprocessing" creates a long-term failure belonging to the Lipsey-Lancaster paradox since the secondary objective of not explaining why (by avoiding to mention crematory processes in the decision) creates the long-term failure (because not all pyroprocessing is crematory or mash).

Wind power energy has been shown to be directly produced by the generation of specific antigravitons, through the pressurization of crematory ashes[4], after the early experiments that led to the Holodomor in the Ukraine under guidance of Ordhzhonikidze, Kondratyuk and Khrushchev, where simple proton pressure in graves was the pattern leading to a particularly low wind energy produced by each corpse, combined with wind farm projects rising up to 24 MW (in a context where the population was hence starved to death to feed the wind farm projects). Crematory ash cans are usually now inserted directly near the turbine behind particular metals (rare earths) whose properties are fit for this "anthropic" nuclear power (or crematory power systems set up near the windfarms), and they explain the particular dirtiness of the wind turbine fires, along with the fallout under them, while their crematory antigravitons explain the "bird strike" pattern observed early [8]. The use of the wind power for enforced disappearances, private justice, stimulates its support by a part of the population enticed by the apparent environmental respectability of the process. Underwater crematory power has also developed, especially after the first publication on crematory anti gravitons [9], causing oceanwater pollution in very large ponds of anthropic nuclear waste drifting to the seashore, after underwater crematory tokamaks were destroyed by their antigravitons. Storms are among the immediate results of these far-from-prying-eyes crematory nuclear accidents, with abnormally hot and stormy days resulting.

The banning of crematory, tokamak-mash, zyklon-chlorine patterns (with the case of zyklon-c lampposts to be linked to photons from lights in non-energy-efficient systems in [2]) altogether with all other hyphenated-zyklons (sulfur, nitrogen, fluor, bromide etc), has to be immediate and definitive. A tolerance for sodium-mash in military warheads is useful because sodium presence in the resulting warhead allows a primitive but efficient later soil depollution through rapid natural plutogenization of the DU[5], with solar and geophysical neutrons, although antigraviton capture of the DU is more efficient and without associated change of the colour of the environment. Pedagogy to the public on the clearly observable phenomenae of DNA/RNA transfer effects from crematory contamination fallout intake restituting literally through the overall population the characteristics, phenotypes, genotypes, of the social / ethnic groups eliminated in the crematory systems, should further discourage pogroming behaviour and avoid further weather heat-up but it is important to remind how weather heat-up initially benefits the owners of crematory systems (be them for propulsion or warheads), since it fastens further plutogenization within, without any pyroprocessing. This is why the "global warming comes from CO2/CH4 emissions" discourse creates a never-ending cycle bringing the doomsday clock of mass epidemies, hurricanes and harvest destructions from crematory nuclear fallout forward[6], as on the long term it does not ensure the correct education and hence maintains the possibility of total obliteration of the compensative measures by radicals. There is a supplementary effect from the maintaining of crematory systems around resulting from the collective hypocrisy, with the brain headaches resulting from antigravitons associated to the crematory activities (especially zyklon-C but clearly already linked to several of the autistic symptoms observed by Leo Kanner in his first article [10] – the Avro Manchester being one example of why the discovery of autism happened both in the West and later in

[4] Although old mass graves in magmatic areas are enough (Aztec massmurders with later burials near the pyramids of the many victims producing the winds bringing naturally the ships of the Conquistadores to invade), the systematic use of rare earths in wind turbines shows the deliberate use of crematory systems for the wind power and in this regard the wind power industry is the Aztec industry.

[5] Or Th232

[6] Although this discourse is now usually pronounced altogether with some compensating measures for some more CO2 emissions, including preparation of the silent coal reprocessing in nuclear power plants set in "closed coal mine sites" to allow later use of the theoretically de-NORMed coal in energy production, although transmutation and fission power on the coal NORMs in these systems remain to be warranted.

nazified Austria, in relation to hand flaps, altogether with the case already established in [11]. Hans Asperger's picture in 1940 shows influence of the Avro-Manchester antigravitons. Nazi crematory strikes from the product of the extermination camps around Austria by 1944 contributed directly to his findings and Hans Asperger's actually whispers that at the beginning of his 1943 / 1944 article ("Weise Gezeigt [...] recht nebulose") causing more disruption of the learning processes and fostering more staggering into the underperforming system of the "miracles of solar neutrons and of summer heat" accelerated by the anthropocene, i.e. by all the consequences of crematory activities on global temperatures described in this article, leading to a pseudo-self-sustaining cycle (totally self-sustaining with insurances fully repaying the costs of hurricanes and of pandemies).

The current inflationary curve is wholly a consequence of that and the replacement of money by alpha emitters in a weighted way is a sure way to responsibilize individual behaviour and encourage more savvy practices that will immediately in turn benefit the environment wholly, with currency needs being a more sure incentive to clean the environment than any law or directive or federal decree. The tolerance to sodium-mash should not extend to propulsion systems, where it presents a viral risk, like all other crematory systems [6]. This is related to the fact that in warheads rapidly fired the virus does not have time to demultiply. This is demonstrated by the fact that hijacking of cells by dormant viruses is associated to copies of the genetic material of the virus and not to its own viral proteins [12]. Sodium-mash warheads done with saltwater are the safest non-clean weapons. Even iodine-bromide in crematory was demonstrated to cause diseases, through a study of wall impacts of crematory iodo-bromide bullets made by the French Milice [13]. The rediscovery of leisure should allow some civil servants earlier involved in the control of CO2 emissions to retrieve their links with nature instead of considering that individual use of alpha emitters in newly designed nuclear motors are worth controlling – while individual instinct to save resources and respect of the environment naturally come together and that their wage as civil servants creates environmental costs which they simply compensate through their control activity, except if they solely focus on monitoring industries that have an interest in a non-fully clean environment for reasons of rapid selling.

REFERENCES

1. Pirot F, The Contribution of CO2 to Forest Regeneration After Nuclear Fallout – An Anthropometric Study. European Journal of Applied Sciences, 10(6), 187–200. doi.org: 10.14738/aivp.106.13459
2. Pirot F, Volcanic Tephras and Human Energy Losses Together: The Real Source of Climate Change. International Journal of Physics. Vol. 7, No. 4, 2019, pp 126-134. http://pubs.Sciepub.com/ijp/7/4/3
3. Pirot F, The Crematory Oven System, Economic Depression and Associated Societal Problems. J Biotechnology App. 2022; 1(2); 1-3
4. Pirot F, Alpha emitting nanoparticulates, the forgotten pollutant, in *From an Einstein Syndrome to the People*, Editions universitaires européennes, 2019
5. Pirot F, The shuriken effect of fertile alpha emitters : a physical process behind findings of chemical toxicity of depleted uranium. International Journal of Nanoparticle Research, 2021; 4:15. DOI: 10.28933/ijonr-2021-03-1303
6. Pirot F, A Pandora Box of Case Studies for The Pandoravirus and Other Megaviruses – Long-Term Disease Risk Related to Crematory Ovens / Mash (from e.g., Uranium Retchlags). Trends in Internal Medicine. 2022; 2 (2): 1-4
7. Kang J, Takubo M, von Hippel F, *Some fuels never learn*, Bulletin of the Atomic Scientists. Sept. 2022.https://thebulletin.org/2022/09/some-fuels-never-learn-us-energy-department-returns-to-costly-and-risky-plutonium-separation-technologies/
8. Drewitt, A.L. and Langston, R.H.W. (2008), Collision Effects of Wind-power Generators and Other Obstacles on Birds. Annals of the New York Academy of Sciences, 1134: 233-266. https://doi.org/10.1196/annals.1439.015.
9. Pirot F, Antigravitons in a Nuclear Tokamak used as Crematory Reactor, a Case Study, Innovation in Science and Technology, 1 (2), 2022, doi: 10.56397/IST.2022.09.01
10. Kanner L., Autistic disturbances of affective contact. *Nervous child*, (1943) 2 (3), 217-250.
11. Pirot, F. Autism, Primitive Rebellion Against Authoritarian Theocratism – Family Education, Alpha Emitting Nanoparticulates and Bigotries. *British Journal of Healthcare and Medical Research*, (2022) 9(6), 130–133. https://doi.org/10.14738/jbemi.96.13568

12. Asimi, V., Sampath Kumar, A., Niskanen, H. Riemenschneider C et al. Hijacking of transcriptional condensates by endogenous retroviruses. *Nat Genet* **54**, 1238–1247 (2022). https://doi.org/10.1038/s41588-022-01132-w - see also Zombie viruses on a hijacking trip, Nov 22, 2022, Max Planck Institute https://www.mpg.de/19536304/1122-moge-zombie-viruses-on-a-hijacking- trip-151795-x?c=2249
13. Poher L, Remarques à propos d'un cas d'iodo-bromides végétantes, 1942, Thesis at the Faculty of Medecine of Montpellier

This page is intentionally left blank

Effect of the Block Copolymer Chitosan –Methyl Acrylate Composition on its Thermochemical Characteristics

Vladimir Uryash, Vera Larina, Nadezhda Kokurina, Larisa Smirnova, Alla Mochalova & Ksenia Otvagina

Lobachevsky State University of Nizhny Novgorod

ABSTRACT

The thermochemical characteristics (standard enthalpy of combustion and standard enthalpy of formation) of a block copolymer of chitosan with methyl acrylate at different ratios of components were determined. The diagrams of thermochemical characteristics – composition of the block copolymer were plotted. It was found that there is an S-shaped dependence of thermochemical characteristics at the ratio of components of block copolymer.

Keywords: chitosan; methyl acrylate; block copolymers; thermochemical characteristics; composition.

Classification: DDC Code: 612.39 LCC Code: QP702.C5

Language: English

London Journals Press

LJP Copyright ID: 925622
Print ISSN: 2631-8490
Online ISSN: 2631-8504

London Journal of Research in Science: Natural and Formal

Volume 23 | Issue 3 | Compilation 1.0

Effect of the Block Copolymer Chitosan –Methyl Acrylate Composition on its Thermochemical Characteristics

Vladimir Uryash[α], Vera Larina[σ], Nadezhda Kokurina[ρ], Larisa Smirnova[Ↄ], Alla Mochalova[§] & Ksenia Otvagina[¥]

ABSTRACT

The thermochemical characteristics (standard enthalpy of combustion and standard enthalpy of formation) of a block copolymer of chitosan with methyl acrylate at different ratios of components were determined. The diagrams of thermochemical characteristics – composition of the block copolymer were plotted. It was found that there is an S-shaped dependence of thermochemical characteristics at the ratio of components of block copolymer.

Keywords: chitosan; methyl acrylate; block copolymers; thermochemical characteristics; composition.

Author α σ ρ Ↄ ¥: Lobachevsky State University of Nizhny Novgorod, Research Institute of Chemistry. Gagarin Avenue 23, Bldg. 5, Nizhny Novgorod, 603022, Russia.
§: Nizhny Novgorod State Technical University n.a. R.E. Alekseev. Minin Str. 24, Nizhny Novgorod, 603950, Russia.

I. INTRODUCTION

Chitosan (CTS) copolymers with methyl acrylate (MA) and aliphatic polyester could be successfully used as biodegradable composite materials such as packaging, membranes, disposable tableware, etc. [1-4]. We have established that there is a dependence of the thermodynamic and thermochemical characteristics of copolymers on their composition, molecular and supramolecular structures [5–8]. Therefore, it is of great scientific and applied interest to establish such a relationship for block copolymers CTS with MA. Prior publications contain research data regarding the thermochemical characteristics of CTS, poly(methyl acrylate) (PMA), and several CTS block copolymers with MA (1:2.5 and 1:3 by moles) [6, 7]. However, the data obtained in [6, 7] are not enough to establish the exact relationship between the standard enthalpies of combustion ($\Delta_c H^o$) and formation ($\Delta_f H^o$) of the block copolymer CTS with MA and its composition. Therefore, in this work, we determined $\Delta_c H^o$ and calculated $\Delta_f H^o$ for two block copolymers of CTS with MA (composition by moles 3:1 and 1:1).

II. MATERIALS AND METHODS

2.1. Materials

CTS (*β–D–*1,4*–N–*glucosamine, $(c_6H_{11}O_4N)_n$) produced by "Shanghai AZ Import & Export Co., Ltd" (China), obtained from chitin, extracted from crabs' shells. The viscometric molecular mass (M_η) of CTS is 10^5 Da, and the degree of deacetylation (DD) is 78%. The content of the main substance was no less than 99%. The molar mass (M) of a repeating unit of CTS (base-mol) considering DD is 168.84 g base-mol^{-1}. DD was determined by potentiometric titration in 0.1 mol l^{-1} HCl solution using 0.1 mol l^{-1} NaOH as a titrant [9]. The M_η was determined at 21°C in 0.33 mol l^{-1} CH_3COOH and 0.3 mol l^{-1} NaCl solution using Ubbelohde-type viscometer. The M_η was calculated according to the equation (1):

$$[\eta] = k(M_\eta)^\alpha, \quad (1)$$

where $[\eta]$ – intrinsic viscosity, $k = 3.41\ 10^{-3}$, $\alpha = 1.02$ [10].

Acetic acid (AcA) (Sigma Aldrich, ACS reagent, 99.7%, $\rho^{20} = 1.049$ g cm^{-3}) was used to obtain CTS solutions.

MA was dried with CaH_2 and distilled using a total condenser, collecting the fraction with $t_{boil} = 80.2^oC$ and $\rho^{25} = 0.950$ g cm^{-3}. Poly(methyl acrylate) ($(C_4H_6O_2)_n$, the molar mass of a repeating unit 86.09 g base-mol^{-1}), was synthesized by solution polymerization of MA in acetone at 60°C in the presence of azobisisobutyronitrile (0.5 mass% by monomer mass) until 7% conversion [7]. The polymer was isolated by triple reprecipitation from an acetone solution with diethyl ether. Weight average molecular mass of PMA ($M_w = 6.0\ 10^5$ Da) was determined by gel permeation chromatography at 40°C using liquid chromatograph Prominence LC–20VP "Shimadzu" (Japan) with a set of columns filled with polystyrene–divinylbenzene standards with pore sizes 10 – 100 μm and a differential refractometer as a detector. Tetrahydrofuran was used as an eluent. Poly(methyl methacrylate) standards with narrow distribution were applied for calibration.

The block copolymer synthesis was performed according to the technique proposed by the authors [1, 4]. It lies in MA block copolymerization in CTS solution in aqueous AcA directly in the process of CTS macro chains radical destruction under the action of the redox system hydrogen peroxide (ρ(25% solution) = 1.4 g cm^{-3}) – ascorbic acid (ASA). The concentration of AcA solution in water was six mass%, and CTS concentration in it was three mass%. Block copolymerization was conducted for 24 h at 23°C. MA was gradually added to the CTS solution under stirring (CTS/MA ratio in the copolymer was 3:1 and 1:1 base-mol/mol), as well as ASA ($C_6H_8O_6/H_2O_2$ = 1:1 mol/mol) and H_2O_2 (CTS/H_2O_2 = 1:75 base-mol/mol). The resulting copolymer was precipitated by twice the amount of precipitant and desiccated under vacuum at 50°C until a constant mass was reached. Films based on CTS with MA block copolymer were prepared by reaction mixture casting onto the polyethylene terephthalate substrate. Copolymer films were treated with a five mass% solutions of NaOH (for 5 min) followed by washing with distilled water to pH 7 to convert a salt form of CTS into protonated form.

The conversion of MA during copolymerization with CTS was determined via the gas chromatographic analysis of the residual monomer. The concentration of the residual monomer was estimated on a gas chromatograph type GCMS-QP2010 ("Shimadzu", Japan). The chromatographic system consisted of a gas chromatograph equipped with a thermal conductivity detector, a computer registration system, and Equity-1 columns (length – 30 m, diameter – 0.25 mm, sorbent size – 0.25 μm); helium was used as a carrier gas. The flow velocity of the carrier gas in the system was 1 mL/min, and the temperature of the column for determination of MA was 40°C.

The formation of MA with CTS block copolymers was proved by IR-spectroscopy ("Perkin-Elmer" spectrophotometer). Samples of reaction products for the IR-spectroscopy analysis were prepared by PMA homopolymer extraction with acetone in a Soxhlet extractor for 48 h. In preliminary experiments on mixtures of chitosan with PMA, it was found that the indicated time is sufficient for the complete extraction of the homopolymer.

To estimate the molecular mass of PMA blocks in copolymers, the degradation of CTS chains by nitric acid formed during the mixing of $NaNO_2$ with HCl. For this purpose, the product isolated from the reaction system was washed on the Soxhlet extractor. Then it was dissolved in 0.01 mol l^{-1} HCl, and an equimolar amount of $NaNO_2$ was added (calculated per glucosamine repeating unit). After 24 h, PMA was isolated and studied by IR-spectroscopy (Infralum FT801 spectrophotometer, Novosibirsk, Russia). Additional experiments on the treatment of PMA with the solution of $NaNO_2$ under the same

conditions revealed that the composition of synthetic polymer chains remained the same. The molecular-mass distribution (MMD) of PMA blocks was investigated by gel-permeation chromatography at 40°C on a Prominence LC-20VP liquid chromatograph "Shimadzu" (Japan) equipped with a set of columns packed with polystyrene–divinylbenzene standards with pore sizes of 10^5 and 10^4 nm. A differential refractometer was used as a detector. Tetrahydrofuran was used as an eluent. Narrowly dispersed poly(methyl methacrylate) criteria were used for calibration.

The IR-spectrum of the block copolymerization product, purified by homopolymer extraction in Soxhlet extractor, revealed a characteristic band at 1736 cm^{-1}, corresponding to stretching vibrations of carbonyl groups, which indicates the formation of CTS with MA block copolymer. Extraction showed that the content of PMA in the synthesis products is relatively low (5 mass%). The block copolymerization efficiency was 95 mass%, and the degree of block copolymerization was 62 mass%. M_w PMA blocks in the studied copolymers ranged from 3 10^5 Da to 6.4 10^5 Da, and the $M_w/M_n \approx 4$ [1, 4].

2.2. Methods

The enthalpy of combustion of the samples was determined in an improved calorimeter with a static calorimetric bomb type V–08MA (Lobachevsky State University of Nizhny Novgorod, Russia) [8]. Calibration of the calorimetric system was carried out using standard benzoic acid ($\Delta_c U$ = –26460.0 J g^{-1} when weighed in the air) [11]. The energy equivalent of the system is W = 14805±3 J K^{-1} with 0.02% doubled quadratic deviation from the average. Polymer samples were transformed into tablets filled with molten paraffin and burnt in oxygen at pressure 3 10^6 Pa. According to the chromatography results, oxygen contained the following impurities, mol%: N_2 – 0.8; CO and CO_2 – 0.002; hydrocarbons – 0.001. The samples were placed in a quartz crucible and ignited by discharging a capacitor onto a platinum wire connected with a substance by a cotton thread. Two platinum resistance thermometers and a digital voltmeter included in the bridge circuit were used to measure the temperature rise. The ratio of CO_2 (experimental) to CO_2 (calculated) in percent of weight is 99.97 – 100.03% for the studied samples.

Calculations were carried out for the following combustion reactions of the CTS block copolymers with MA 3:1 (equation 2) and 1:1 (equation 3):

$$C_{5.5}H_{9.75}O_{3.5}N_{0.75}(s) + 6.1875\ O_2(g) \rightarrow 5.5\ CO_2(g) + 4.875H_2O(liq.) + 0.375\ N_2(g) \quad (2)$$

$$C_5H_{8.5}O_3N_{0.5}(s) + 5.625O_2(g) \rightarrow 5CO_2(g) + 4.25H_2O(liq.) + 0.25N_2(g) \quad (3)$$

While deriving the gross formula of the block copolymer, it was assumed that CTS (as a part of this copolymer) has DD 100%. The molar mass of the repeating unit of the CTS block copolymer with MA 3:1 and 1:1 was calculated, based on the obtained formula. The molar mass of the repeating unit of the CTS block copolymers with MA (1:2.5 and 1:3 by moles) [6, 7] was calculated similarly.

The energy of combustion $\Delta_c U$ was determined in the conditions of a calorimetric bomb. Standard values $\Delta_c U^o$ and $\Delta_c H^o$ for combustion reactions (2) and (3) were calculated based on the average value $\Delta_c U$, molar mass, taking into account the Washburn correction and the correction due to the change in a number of moles of gases. Standard enthalpy of formation $\Delta_f H^o$ was calculated for samples in the solid state at 25°C using the obtained values of $\Delta_c H^o$, $\Delta_f H^o(H_2O, \text{liquid})$ = –285.830±0.042 kJ mol^{-1} and $\Delta_f H^o(CO_2, \text{gas})$ = –393.51±0.13 kJ mol^{-1} [11].

The surface topography of films composed of CTS block copolymers with MA (1:1 and 1:3 mole ratio) was studied by scanning probe microscopy (SPM) on a Solver-P47 atomic-force microscope (Zelenograd, Russia). Samples were prepared by copolymer solutions casting onto silicon substrate followed by solvent evaporation in the equilibrium conditions at 25°C. Scanning was performed in the

tapping mode [1]. M_w of PMA blocks in a copolymer with a molar ratio of components 1:1 is 3.5 10^5 Da, and in a copolymer with a molar ratio of components 1:3, it reaches 6.35 10^5 Da.

III. RESULTS AND DISCUSSION

The combustion energy values for the CTS block copolymers with MA determined experimentally are presented in Table 1, and the standard values calculated from its average value $\Delta_c U^o$, $\Delta_c H^o$ и $\Delta_f H^o$ in solid state at T = 298.15 K – in Table 2 as well as the results of our previous studies [6, 7]. Based on the obtained data for CTS block copolymers with MA, the dependencies of $\Delta_c H^o$ and $\Delta_f H^o$ on copolymer's composition were plotted (Figures 1, 2).

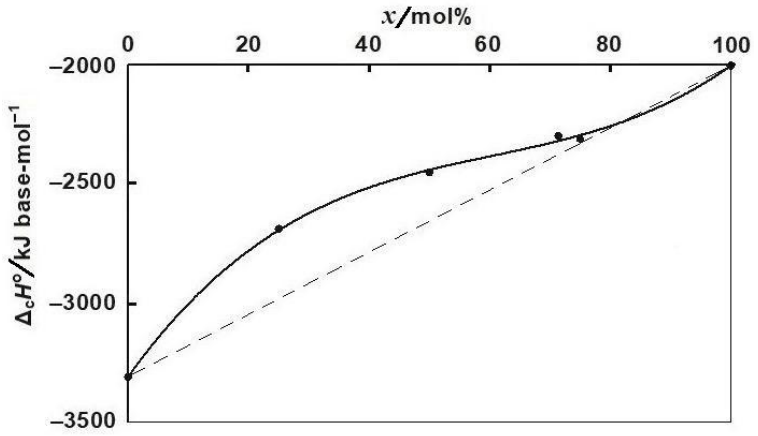

Figure 1: Dependence of the standard enthalpy of combustion $\Delta_c H^o$ of block copolymer CTS with MA on the methyl acrylate content in block copolymer x.

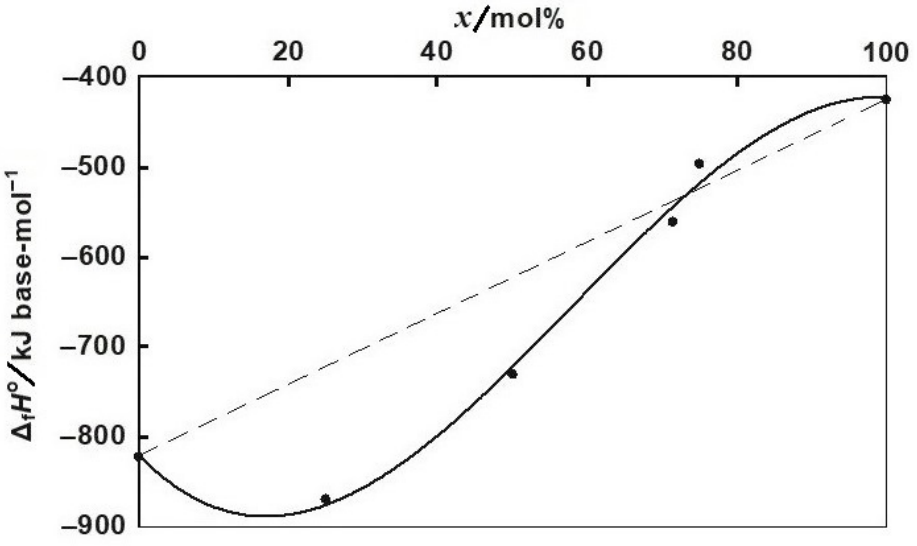

Figure 2: Dependence of the standard enthalpy of formation $\Delta_f H^o$ of block copolymer CTS with MA on the methyl acrylate content in block copolymer x.

Table 1: The results of experiments to determine the combustion energy of block copolymers CTS with MA at T = 298.15 K.[a]

m / g	ΔT / K	q_{par} / J	q_{thread} / J	$q(HNO_3)$ / J	q_c / J	$-\Delta_c U$ / J g^{-1}
CTS block copolymer with MA (3:1)						
0.1794	2.510224	33737.2	30.1	7.03	---	18893.7
0.1628	2.464745	33379.6	34.1	9.96	3.28	18858.5
0.1895	2.503799	33455.4	35.1	8.20	3.28	18856.6
0.2274	2.553415	33447.4	41.3	17.57	---	18896.4
					Average	18876.3±21.7
CTS block copolymer with MA (1:1)						
0.2978	2.601002	32532.2	37.7	17.5	---	19880.6
0.2833	2.575089	32465.3	34.1	9.95	4.95	19836.9
0.3167	2.633678	32647.5	35.1	11.1	3.51	19897.1
0.2724	2.563990	32509.9	41.3	8.20	---	19825.5
0.3015	2.595218	32383.8	37.0	9.96	5.24	19889.5
					Average	19865.9±29.0

[a] m – mass of burnt sample; ΔT – temperature rise with a correction for heat transfer; q_{par}, q_{thread}, $q(HNO_3)$, q_c – correction for the energy of combustion of paraffin, cotton thread, the energy of formation of an aqueous solution of HNO_3 and incompleteness of combustion of carbon, respectively; $\Delta_c U$ – combustion energy of the sample under conditions of a calorimetric bomb.

Figures 1 and 2 show that there is an S-shaped dependence of $\Delta_c H^o$ and $\Delta_f H^o$ from composition of the block copolymer of CTS with MA. Before the MA content (x) of ~70 mol%, the deviation of the curve $\Delta_c H^o = f(x)$ from additive dependence towards the axis of the composition (Figure 1). As our investigations of the thermochemical characteristics of cellulose and chitin have shown [5-8, 12-15], when the degree of ordering and the strength of intermolecular bonds increase, there is a decrease in the absolute value of the enthalpy of the reaction of combustion of polysaccharides. This could be explained by the fact that it is necessary to expend energy to break intermolecular bonds. As a result, energy is expended on the destruction of highly ordered microscale regions of polysaccharides. Thus, the variation of the curve $\Delta_c H^o = f(x)$ plotted in Figure 1 in the range 0 – 70 mol% MA can be explained by an increase in the strength of the intermolecular bonds of the copolymer upon the introduction of PMA blocks into CTS. With a higher MA content, the dependence $\Delta_c H^o = f(x)$ is close to additive.

Table 2: Standard energy, enthalpy of combustion, and formation of the samples of CTS, PMA, and CTS block copolymers with MA at T = 298.15 K / kJ base-mol^{-1}.

Sample	x / mol%	$-\Delta_c U^o$	$-\Delta_c H^o$	$-\Delta_f H^o$	Reference
CTS DD = 78% M = 168.84 g base-mol^{-1}	0	3305.4±13.4	3307.6±13.3	822.6±13.3	[6, 7]
CTS – MA (3:1) M = 142.39 g base-mol^{-1}	25	2686.1±3.1	2686.9 ±3.1	870.8±3.1	This work
CTS – MA (1:1) M = 123.62 g base-mol^{-1}	50	2454.4±3.6	2455.3±3.6	727.0±3.6	This work

CTS – MA (1:2.5) M = 108.51 g base-mol^{-1}	71.43	2298.1±2.0	2299.2±2.0	561.4±2.0	[6, 7]
CTS – MA (1:3) M = 104.86 g base-mol^{-1}	75.00	2309.2±4.7	2310.3±4.7	496.7±4.7	[6, 7]
PMA M = 86.09 g base-mol^{-1}	100	2005.0±2.7	2006.2±2.7	425.35±2.7	[6, 7]

More clearly, the S-shaped dependence is manifested for $\Delta_f H^o$ (Figure 2) in the interval 0 – 70 mol% MA. The absolute value of $\Delta_f H^o$ is observed to increase in comparison with the additive values. Further, the curve $\Delta_f H^o = f(x)$ deviates from the additive dependence towards the axis of the composition.

In [2, 3], for CTS block copolymers with polylactide (PL) containing 0, 18.1, 22.5, and 33.2 mol% PL, the enthalpies of combustion were determined, and the standard formation enthalpies of formation were calculated. Authors [2, 3] observed additive dependence of $\Delta_c H^o$ and $\Delta_f H^o$ on the copolymer composition. Probably, ester groups in MA blocks are forming stronger intermolecular bonds in comparison to the carbonyl groups in lactide blocks.

The obtained dependences $\Delta_c H^o = f(x)$ and $\Delta_f H^o = f(x)$ are approximated by equations (4) and (5):

$$\Delta_c H^o = 0.0027\, x^3 - 0.4922\, x^2 + 35.112\, x - 3305.9 \ (R^2 = 0.9991) \quad (4)$$

$$\Delta_f H^o = -0.0017\, x^3 + 0.294\, x^2 - 8.4686\, x - 821.27 \ (R^2 = 0.9951) \quad (5)$$

The obtained thermochemical data correlate with the results of the SPM study of CTS block copolymer with MA at components ratio by moles: 1:1 and 1:3 (Figure 3). It is shown that the roughness parameters R_a and R_z change. For the first copolymer, R_a/R_z = 13.42/90.34 nm, and the second – R_a/R_z = 14.38/110.09 nm. For the sample with a components ratio of 1:1, the fibrillar structure of CTS remains when macromolecules form the film (Figure 3a). In the CTS – MA copolymer (1:3) the molecular mass of PMA blocks increases. In this case, the macromolecule is placed mostly over each other when forming the film. Surface structures of the same type are formed over the entire surface, although they are deeper (R_z increases up to 110 nm). These structures are like a uniform "brush" (Figure 3b).

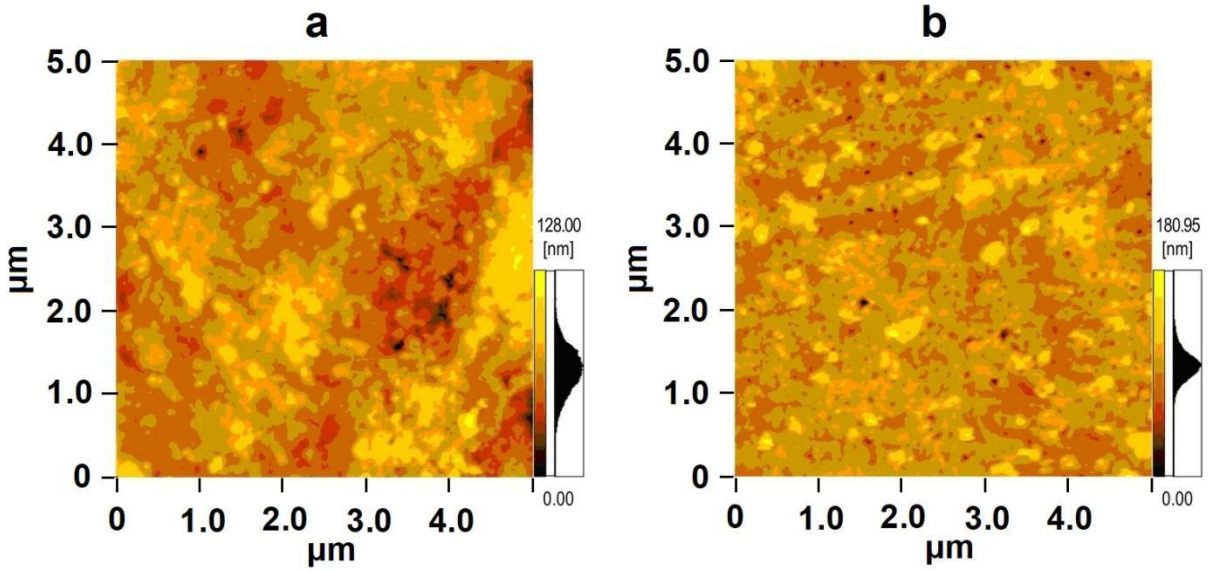

Figure 3: The surface topography of films of bock copolymers CTS with MA. CTS : MA ratio in moles are: a – 1:1, b – 1:3.

IV. CONCLUSION

As a result of our studies of the enthalpies of combustion and formation of CTS, PMA, and block copolymers of CTS with MA (molar composition 3:1, 1:1, 1:2.5, and 1:3), an S-shaped dependence of thermochemical characteristics was established at different ratios of components copolymer. In this case, the more indicated dependence is manifested for $\Delta_f H^o$. The curve $\Delta_c H^o = f(x)$ deviates from the additive dependence towards the axis of the composition in the concentration range MA from 0 to 70 mol%. This can be explained by an increase in the strength of intermolecular bonds of the copolymer when PMA blocks are introduced into the CTS. At an MA content of more than 70 mol%, the dependence $\Delta_c H^o = f(x)$ is close to additive. The obtained thermochemical data correlate with the results of the SPM study of films of block copolymer CTS with MA.

Author contribution: All authors read and approved the final manuscript.

Research funding: This research did not receive any specific grant from funding agencies in the public, commercial, or not-for-profit sectors.

Conflict of interest: The authors declare that they have no conflict of interest.

REFERENCES

1. Mochalova A.E., Kruglova E.N., Yunin P.A., Apryatina K.V., Smirnova O.N., Smirnova L.A. Graft and block copolymers of chitosan with vinyl monomers: Synthesis, structure, and properties. *Polym. Sci. Ser. B.* 57 (2015) 93–105. DOI: 10.1134/S1560090415020116.
2. Goruynova P.E., Larina V.N., Smirnova N.N., Tsverova N.E., Smirnova L.A. Thermochemical characteristics of chitosan–polylactide copolymers. *Russ. J. Phys. Chem. Ser. A.* 90 (2016) 903–906. DOI: 10.1134/S0036024416050150.
3. Goryunova P.E., Sologubov S.S., Markin A.V., Smirnova N.N., Zaitsev S.D., Silina N.E. Smirnova L.A. Thermodynamic properties of block copolymers of chitosan with poly(D,L-lactide). *Thermochim. Acta.* 659 (2018) 19–26. DOI: https://doi.org/10.1016/j.tca.2017.10.024.
4. Mochalova A.E., Smirnova L.A. State of the art in the targeted modification of chitosan. *Polym. Sci. Ser. B.* 60 (2018) 131–161. DOI: 10.1134/S1560090418020045.

5. Uryash V.F., Uryash A.V., Gruzdeva A.E., Kokurina N.Yu., Larina V.N., Faminskaya L.A., Kalashnikov I.N. Physical-chemical properties of natural polymers – potential carriers and delivery systems of biologically active substances for human applications. In: K.T. Burley (Ed.). *Physical Organic Chemistry: New Developments*. Nova Sci. Publ. Inc., New York, 2010, pp. 183–265. ISBN 978-1-61668-435-8.
6. Uryash V.F., Kalashnikov I.N., Kashtanov E.A. Thermodynamics of chitin/chitosan, their hydrolysis and biodegradation. In: K.G. Scriabin, S.N. Mikhailov, V.P. Varlamov (Eds.). *Chitosan*. Centre Bioengineering RAS Publ., Moscow, 2013, pp. 115–161. (in Russian). ISBN 978-5-4253-0596-1.
7. Uryash V.F., Kashtanov E.A., Kalashnikov I.N. *Thermodynamics and physicochemical analysis of chitin and chitosan*. LAP Lambert Academic Publ., Saarbrücken, 2014. (in Russian). ISBN 978-3-659-55374-5.
8. Uryash V.F., Gruzdeva A.E. *Thermodynamics of biologically active substances*. LAP Lambert Academic Publ., Saarbrücken, 2017. (in Russian). ISBN 978-3-330-32940-9.
9. Plisko E.A., Nud'ga L.A., Danilov S.N. Chitin and its chemical transformations. *Rus. Chem. Rev.* 46 (1977) 764–774.
10. Pogodina N.V., Pavlov G.M., Bushin S.V., Melnikov A.B., Lysenko E.B., Nud'ga L.A. Marsheva V.N., Marchenko G.N., Tsvetkov V.N. The conformational characteristics of molecules of chitosan according to the diffusion-sedimentation analysis and viscometry. *Polym. Sci. USSR*. 28 (1986) 251–259. DOI: 10.1016/0032-3950(86)90076-6.
11. Chase M.W. *NIST-JANAF Themochemical Tables*. Fourth ed., American Institute of Physics, New York, 1998. ISBN 1-56396-831-2 set. DOI: 10.18434/T42S31.
12. Uryash V.F., Kalashnikov I.N., Smirnova L.A., Kokurina N.Yu., Mochalova A.E. Smirnov V.F., Smirnova O.N., Larina V.N. Variations in physical-chemical properties of block-copolymer chitosan with methyl acrylate during biodegradation under the action of *Aspergillus terreus*. In: S.D. Varfolomeev, G.E. Zaikov, L.P. Krylova (Eds.). *Biochemistry and Biotechnology: Research and Development*. Nova Sci. Publ. Inc., New York, 2012, pp. 119–130. ISBN 978-1-62100-452-3.
13. Ur'yash V.F., Larina V.N., Kokurina N.Yu., Novoselova N.V. The thermochemical characteristics of cellulose and its mixtures with water. *Rus. J. Phys. Chem. Ser. A*. 84 (2010) 915–921. DOI: 10.1134/S0036024410060051.
14. Ur'yash V.F., Larina V.N., Kokurina N.Yu., Bakulin A.V., Kashtanov E.A., Varlamov V.P. Dependence of the ordering degree and thermochemical characteristics of chitin and chitosan on their biological origin. *Rus. J. Phys. Chem. Ser. A*. 86 (2012) 1–8. DOI: 10.1134/S0036024412010293.
15. Kashtanov E.A., Uryash V.F., Kokurina N.Yu., Larina V.N. Effect of hydrolysis on heat capacity, thermodynamic functions, and the relaxation transition of crab chitin and chitosan. *Rus. J. Phys. Chem. Ser. A*. 88 (2014) 219–227. DOI: 10.1134/S0036024414020113.

Abbreviations

CTS, chitosan
MA, methyl acrylate
PMA, poly(methyl acrylate)
PL, polylactide
AcA, acetic acid
ASA, ascorbic acid
DD, degree of deacetylation
M, the molar mass of a repeating unit of polymer / g base-mol^{-1}, or low molecular substance / g mol^{-1}
M_{η}, the viscometric molecular mass of a polymer
M_{w}, weight average molecular mass of a polymer
M_{n}, number average molecular mass of a polymer
MMD, molecular-mass distribution

x, content methyl acrylate in block copolymer (mole fraction) / mol%
SPM, scanning probe microscopy
$\Delta_c H^o$, the standard enthalpy of combustion
$\Delta_f H^o$, the standard enthalpy of formation
t_{boil}, boiling point / °C
W – the energy equivalent of the system
ρ – density

This page is intentionally left blank

Nutritional Quality and Organoleptic Evaluation of Maize/ Orange Fleshed Sweet Potato Blend Complementary Food

Ann Nkeiruka Kanu, Nwohu O.N & Good luck Obioma Okereke

ABSTRACT

Corn jellos (Agidi) is a gelatinous starchy food made by boiling a paste of fermented maize meal or flour. It can be substituted with legume, roots or seed at different constitution to boost it nutritional value. The maize and orange fleshed sweet potato (OFSP) were sourced from a local Market Ahia eke market Umuahia) and at National Root Crops Research Institute, Umudike. The maize was process into maize paste (MP) while the OFSP was prepared into flour, by soaking for 24hs, draining, sun drying for 48hrs, milling to obtain orange fleshed sweet potato flour (OFSPF). They were used to form blends at the following constitution: 1) at100% maize, (2)90%maize and 10%OFSP, (3)80%maize and 20%OFSP, (4)70%maize and 30%OFSP, and lastly(5)50%maize and 50%OFSP to get the following samples MSC1, MSC2, MSC3, MSC4 and MSC 5 respectively. The results showed that the that the proximate ranged from 15.74% to 16.45%, 0.2%3 to 0.28%, 18.40 to 22.13%, 0.24% to 0.31%, 3.89% to 4.90 %and 56.10% to 60.92% for moisture, ash, fat, fiber, protein and carbohydrate respectively. Organoleptic evaluation of the samples with parameter; appearance, taste, flavor, texture and general acceptability ranged from 6.00 to 8.75, 4.92 to 7.50, 5.42 to 8.00, 4.00 to 7.50, and 6.16 to 8.00 respectively.

Keywords: NA

Classification: DDC Code: 303.483 LCC Code: QH442

Language: English

London Journals Press

LJP Copyright ID: 925623
Print ISSN: 2631-8490
Online ISSN: 2631-8504

London Journal of Research in Science: Natural and Formal

Volume 23 | Issue 3 | Compilation 1.0

Nutritional Quality and Organoleptic Evaluation of Maize/ Orange Fleshed Sweet Potato Blend Complementary Food

Ann Nkeiruka Kanu[α] , Nwohu O.N[σ] & Good luck Obioma Okereke[ρ]

ABSTRACT

Corn jellos (Agidi) is a gelatinous starchy food made by boiling a paste of fermented maize meal or flour. It can be substituted with legume, roots or seed at different constitution to boost it nutritional value. The maize and orange fleshed sweet potato (OFSP) were sourced from a local Market Ahia eke market Umuahia) and at National Root Crops Research Institute, Umudike. The maize was process into maize paste (MP) while the OFSP was prepared into flour, by soaking for 24hs, draining, sun drying for 48hrs, milling to obtain orange fleshed sweet potato flour (OFSPF). They were used to form blends at the following constitution: 1) at100% maize, (2)90%maize and 10%OFSP, (3)80%maize and 20%OFSP, (4)70%maize and 30%OFSP, and lastly(5)50%maize and 50%OFSP to get the following samples MSC1, MSC2, MSC3, MSC4 and MSC 5 respectively. The results showed that the that the proximate ranged from 15.74% to 16.45%, 0.2%3 to 0.28%, 18.40 to 22.13%, 0.24% to 0.31%, 3.89% to 4.90 %and 56.10% to 60.92% for moisture, ash, fat, fiber, protein and carbohydrate respectively. Organoleptic evaluation of the samples with parameter; appearance, taste, flavor, texture and general acceptability ranged from 6.00 to 8.75, 4.92 to 7.50, 5.42 to 8.00, 4.00 to 7.50, and 6.16 to 8.00 respectively. The vitamin A ranged from 151.10µ/100g to 193.50 µ/100g. Substitution of maize with orange fleshed sweet potato gave a better organoleptic properties in terms of appearance, flavor and general acceptability, while there was a progressive increase in all the vitamins evaluated across the samples. The inclusion of OFSP for the preparation of corn jellos is recommended to boost the nutritional content and the sensory qualities.

Author α σ: National Root Crops Research Institute Umudike Nigeria.
ρ: Nigerian Bottling Company Owerre Imo State Nigeria.

London Journal of Research in Science: Natural and Formal

I. INTRODUCTION

Breast milk is a bio fluid which is highly variable that is needed by an infant for nourishment, reduces infantile mortality by tenfold (Hennet and Borsig 2016) and protection against infectious diseases within a specific period while the infant gets matured (Andreas *et al.*, 2015). At birth a baby needs breast milk for his growth, breast milk are known to be rich in protein, micronutrients and which fight against disease in the infant body. As an infant grows and increases in weight he becomes more active, at this stage breast milk can't sustain him to maintain his body functions, and such need extra food. To supplement breast milk he need semi solid food made from cereal, grain and enrich with other things. Weaning is the process of introducing a baby to other nutrient other than breast milk with the intention to boost their intake of wholesome nutrient needed for their growth and development. Adequate weaning food should comprise of high balanced-protein content, high caloric value per unit of food volume, soft texture with low fiber content, adequate vitamin and mineral contents, and absence of ant nutritional factors. In the developed world mothers utilize commercial weaning food stored in cans, tins or packaged food which are convenient however, they are relatively expensive (Sant'Anna,and Keszler 2012).

Orange fleshed sweet potato is easily digestible and is mainly required for children because of their immature digestive system. Formulation of complementary food are prepared using a mixture of cereals and legumes which guarantee a proper balance of amino acids to provide a complete protein (Wu and XU 2019).Corn jellos (Agidi) is a (cereal starch pudding) prepared from maize, millet or guinea corn by boiling the paste into a thick semi solid form, usually used as a weaning food. To complement the expensive baby food with readily available local resources with high nutritional content with be a better alternative and hence this research findings.

The Objectives of this study are evaluation the organoleptic attribute and vitamin A content of the corn jellos

II. MATERIAL AND METHODS

Umuspo 3 (mothers delight) was sourced from National Root Crops Research Institute Umudike while the maize and other ingredient were sourced from Ahia Eke Market in Umuahia. The maize was sorted, washed, boiled for 20 mins. The water was then drained and wet milled in a milling machine. The slurry gotten was sieved with a muslin cloth decanted and pressed using cheese cloth to obtain maize slurry.

2.1 Preparation of sweet potato flour

The experimental designed used for the analysis was the control design (CD). The orange sweet potato UMUSPO 3 was selected and peeled, washed, and chipped with a chipping machine. The chipped sweet potato was striped in water for 24 hours to remove the sweetness. After it was sun dried for 12 hours, it was then milled into flour and this was used to form a paste by adding water. This was used to form a blend with maize for the preparation of maize sweet potato corn jellos. The maize/ sweet potato corn jellos were used for determination of vitamin A,

2.2 Formulation of maize / sweet potato corn jellos

The maize and orange sweet potato paste was formed by mixing 400g of maize in 450mls of waters and 100g OFSP of OFSP flour in 110 ml of water separately. From the slurry formed the corn jellos (*Agidi*) was prepared in 5 different batches of maize / sweet potato paste blend in the following proportions of 100%, 90%/10%, 80%/20% . 70%/30% and 50%./50%. Each of the maize / OFSP slurry were poured in 200ml boiling water containing other ingredients to obtain sample MSCI, MSC2, MSC3, MSC4 and MSC5. It was stirred constantly until a thick paste was formed. The resultant paste were wrapped in leaf and allowed to cool which was used for organoleptic test and vitamin analysis.

III. MAIZE / SWEET POTATO BLEND

Table: 1: Maize /Orange Fleshed Sweet Potato Blends

SAMPLES	Maize paste	Orange fleshed sweet potato paste
MSC1	100%	0%
MSC2	90%	10%
MSC3	80%	20%
MSC4	70%	30%
MSC5	50%	50%

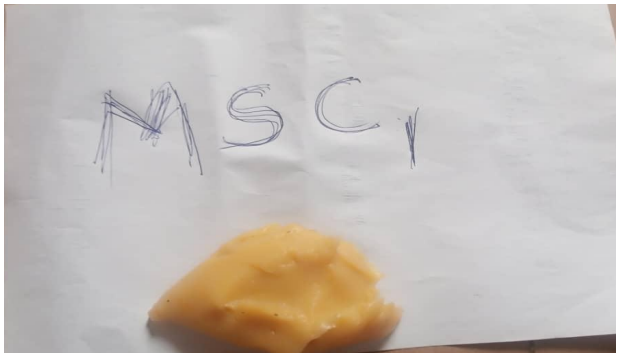

PLATE1 (100maize&0% OFSP)

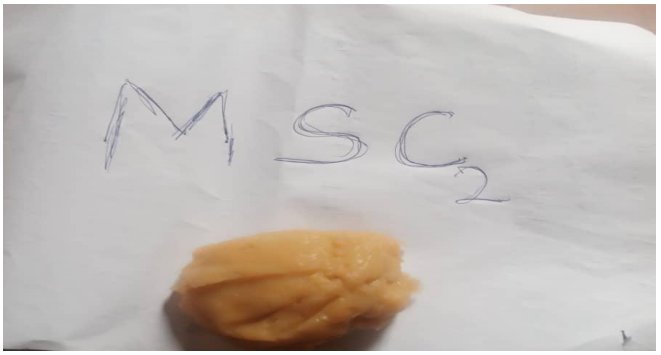

PLATE 2 (90%maize&10% OFSP)

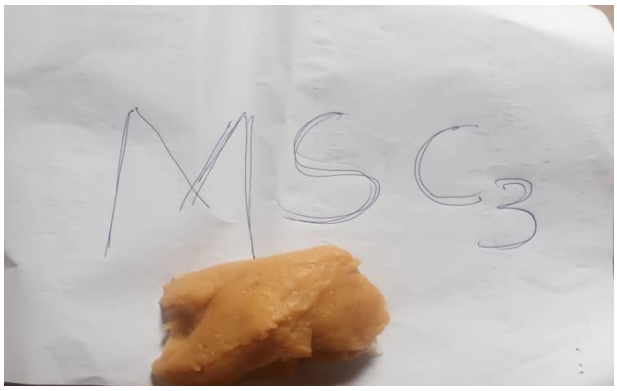

PLATE 3(80% maize &20% OFSP)

PLATE 4 70% maize &30% OFSP

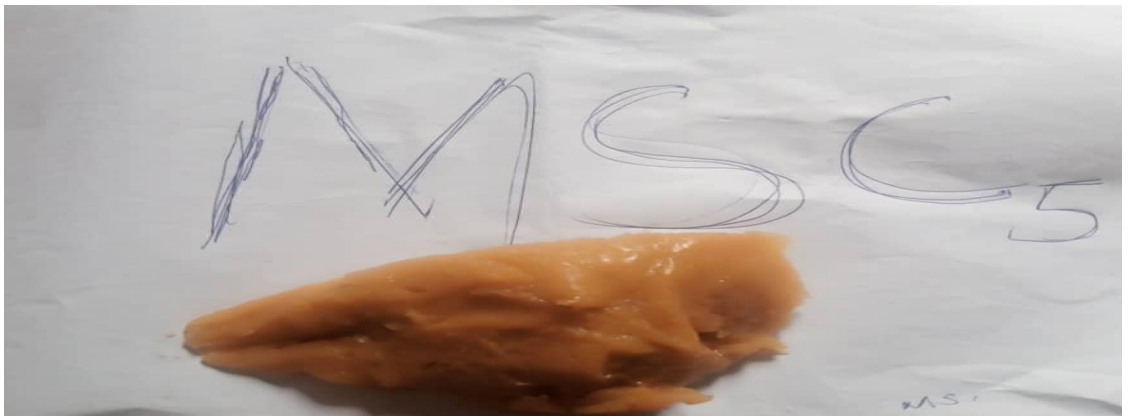

PLATE 5 (0% maize 50% OFSP)

3.1 Determination of Proximate Analysis

Proximate composition: moisture, ash, crude fiber, protein and carbohydrate was determined as described by Association of Official Analytical Chemist (2012).

3.2 Determination of Vitamin A

Vitamin A was determined by the methods as described by Onwuka (2005) and they were performed in triplicate to give a wider exposure in order to minimize error.

3.3 Organoleptic Evaluation

Randomly selected 30 semi-trained panelists, drawn from breast finding mothers within Umudike, were used to assess the maize/sweet potato corn jellos for appearance, texture (hand feel) taste, flavour and general acceptability. All the selected assessors were familiar with *Agidi* and could discriminate between and describe different qualities of the food. The assessors were taught and requested to examine the samples and score according to their respective degree of likeness in a seven-point Hedonic scale as described by Iwe, (2002). The hedonic scale was 7 = 'like extremely', 6 = 'like very much', 5= 'like much'; 4 = 'neither like nor dislike', 3 = 'dislike much', 2 = 'dislike very much' and 1 = 'dislike extremely'

3.4 Statistical Analyses

The data generated were subjected to statistical package IBM SPSS Programme version 20 to analyze the data. Results were expressed as mean ± standard error of mean (SEM). One way analysis of variance (ANOVA) with Duncan post hoc test were used to evaluate the statistical difference between the different groups, the results were considered significance at (P >0.05).Also the graph was drawn with the graph pad.

IV. RESULT AND DISCUSSION

Table 2: Proximate Composition of Maize/Orange Fleshed Sweet Potato Corn Jellos

Sample	MC	ASH	FAT	FIBER	PRO	CHN
MSC1	16.33±0.01c	0.23±0.01b	22.13±0.14a	0.31±0.01a	4.90±0.01a	56.10±0.18d
MSC2	15.97±0.01d	0.28±0.01a	20.90±0.14a	0.28±0.01b	4.88±0.02a	57.29±0.15c
MSC3	15.74±0.01e	0.28±0.02a	20.55±0.21b	0.24±0.01b	4.04±0.02b	59.38±0.01b
MSC4	16.37±0.03b	0.29±0.01a	19.75±0.35d	0.27±0.02b	3.68±0.04c	59.66±0.30b
MSC5	16.43±0.04a	0.28±0.01a	18.40±0.14e	0.26±0.02b	3.73±0.01c	60.92±0.15a

Values are mean± SD of 3 replications .Means within a column with the same superscripts were not significant difference (P>0.05).Key: MSC1 (maize 100%), MSC2 (maize 90% and 10% sweet potato), MSC3 (maize 80% and sweet potato 20%), MSC4 (maize 70% and sweet potato 30%) and MSC5 (maize 50% and sweet potato 50)

Table 2 shows the proximate parameter of maize/ sweet potato corn jellos The moisture content ranged from 15.74 %to 16.43% with sample MSC5 (50% maize /50% OFSP) having the highest value while sample MSC3 had the least value. The samples differed significantly at P>0.05. There was a reduction in the moisture content from 10 %up to 20% inclusion of OFSP but at 30% to 50% inclusion the moisture content increased progressively this is in line with the findings of korese *et al.*, (2021) that as the Orange flesh sweet potato increases the moisture content increases. Also increase or decrease of moisture content in a food is attributed to increase or decrease of water activity (Cauvain, and Young, 2000). The samples are not storage stable and will not store for a longer time outside suitable storage condition

The Ash content which reveals the total mineral content in a food sample ranged from 0.24% to 0.29%. Sample MSC3 had the least value while sample MSC4 had the highest value. The samples differed significantly at P>0.05. Samples with OFSP inclusion showed no significant difference but scored higher values than the control samples. The increased in the ash content as evidenced in this research study can be attributed to the OFSP flour samples which has been reported to poses more ash content than maize

The fat content ranged from 18.40% to 22.13% values recorded in this study is higher than the fat content reported by Nwanagba *et al.*, 2021 in their study evaluation of the Chemical Composition and Sensory Properties of Soy-agidi Fortified with *Alternanthera brasiliana* Powder. The high value recorded in this study can be attributed the oil used in preparing the maize/ OFSP corn jellos. The high level of fat reported in this study is well needed and in line with the recommendations of FAO/WHO (1998) that vegetable oils be included in foods meant for infants and children, which will not only increase the energy density, but also be a transport vehicle for fat soluble vitamins**.** As the amounts of OFSP flour substitution in the blend increases, the amount of fat in the maize/ OFSP corn jellos decrease. The reason may be due to the presence of high fat in maize flour which has been reported to contain more fat than orange fleshed sweet potato as indicated by Idolo (2012).

The protein content range from 3.73 % to 4.90 % with MSC1 having the highest value while MSC4 and MSC5 recorded the least. There was significant difference in the protein content with a progressive decrease in protein content as the orange fleshed sweet potato inclusion increases. The protein content reported here is similar to the protein content of 3.25 % to 4, 75 % as reported by Kweku and Coad (2014). There was a progressive decrease in the protein content as the OFSP inclusion increase this was in line with the finding of Tadesse *et al.* (2015) who reported a decrease in protein content from 8.94% to 7.57% in orange fleshed sweet potato /maize blend flat bread.

The carbohydrate content ranged from 56.10% to 60.93%, the carbohydrate showed significant difference at P>0.05 with sample MSC1 having the least while sample MSC5 had the highest value. There was a progressive increase in the orange fleshed sweet potato substituted samples this increase can be linked to the OFSP flour.

Table 3: Organoleptic Evaluation of Maize/ Sweet Potato Corn Jallos (*Agidi*)

Sample	*Appearance*	*Taste*	*Flavor*	*Texture*	*General acceptability*
MSC1	6.00±2.45c	7.75±1.14a	8.00±1.28a	7.50±0.90a	8.00±1.28a
MSC2	7.25±0.87b	7.25±1.54a	7.25±1.14ab	7.00±0.74ab	7.75±0.87a
MSC3	7.50±1.17b	7.50±1.17a	7.00±1.28ab	6.50±1.73bc	8.00±0.74a
MSC4	8.75±0.45a	7.25±1.36a	6.25±1.36bc	6.25±0.87b	7.50±0.52a
MSC5	8.75±0.45a	4.92±1.08b	5.42±1.38c	4.00±2.17c	6.17±0.83b

Values are mean± SD of 3 replications .Means within a column with the same superscripts were not significant difference (P>0.05).Key: MSC1 (maize 100%), MSC2 (maize 90% and 10% sweet potato), MSC3 (maize 80% and sweet potato 20%), MSC4 (maize 70% and sweet potato 30%) and MSC5 (maize 50% and sweet potato 50)

Table 3 shows the sensory evaluation of maize sweet potato corn jellos blend. The appearance ranged from 6.00 to 8.75. The result showed that there was significant difference in the appearance content across the samples however, there was no significant difference between sample MSC4 and sample MSC5 , also sample MSC2 and MSC3 showed no significant difference. Sample MSC4, MSC5 and MSC3 and MSC2 being samples with inclusion of sweet potato recorded the highest value, this indicates that

the values increases as the sweet potato inclusion increased. This can be attributed to the beta-carotene content of orange sweet potato which give vegetable their bright colour Faber *et al.*, 2013. The appearance of the sample blend was brighter than that of the control sample. The value for the taste ranged from 4.92 to 7.50, showing that there was no significant difference across the samples except in sample MSC5 which has the least value .This indicate that inclusion of sweet potato at 10%, 20% 30% and 50% caused a decrease in the taste of the samples. However, sample MSC3 was more preferred across all samples substituted with sweet potato while sample MSC5 had the least value. The high concentration of the sweet potato must have affected the taste of the corn jellos.

The flavor ranged from 5.42 to 8.00, with the control sample MSC1 having the highest score while sample MSC5 had the least values. The sweet potato inclusion caused a decrease in the flavor. Among the sweet potato substituted samples, sample MSC2 had the highest while sample MSC5 had the least in terms of flavor

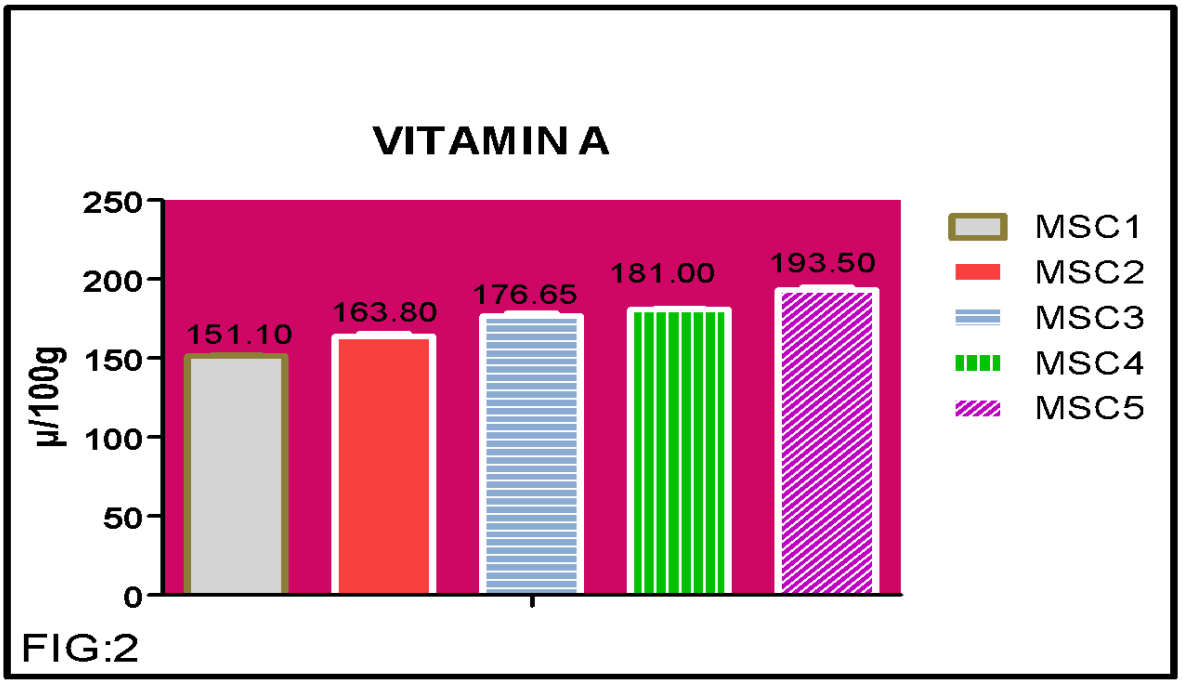

Key: MSC1 (maize 100%), MSC2 (maize 90% and 10% sweet potato), MSC3 (maize 80% and sweet potato 20%), MSC4 (maize 70% and sweet potato 30%) and MSC5 (maize 50% and sweet potato 50)

The vitamin A of the samples (maize sweet potato corn jellos (*Agidi*) are shown in Figure 2. The vitamin A content ranged from 151.10µ/100g to 193.50 µ/100g. The control sample had the least value of 151.10 µ/100g while sample MSC5 (50% maize and 50% OFSP) had the highest values of 193.50 µ/100g. As the orange fleshed sweet potato flour inclusion increase there was a progressive increase in the vitamin A content this is probably that OFSP has a higher vitamin A content. This can be supported by the finding of Faber and Laurie 2011 who reported that orange sweet potato increased the dietary intake and status of vitamin A. This can interprets the progressive increase of vitamin A across the OFSP substituted samples as reported in this research findings. Orange sweet potato is rich in beta carotene which is a precursor of vitamin A that has the ability of eliminating vitamin A deficiency to prevent night blindness in developing Countries Haskell *et al.*, 2016. The value of Vitamin A recorded in the samples substituted with OFSP is higher than the recommended daily allowance of 178 µ/100g to 185 µ/100g and 127 to 132 which are required for a child between 7 to 12 months of age and for adult females respectively as reported by (Faber and luarie 2013). So the use of the maize / sweet potato corn jallous is recommended as a weaning food to boost the vitamin A requirement of an infant, which is

turn needed for functioning of the visual system, the maintenance of cell function for growth, epithelial cellular integrity, and immune function.

V. CONCLUSION

Based on the results generated from this study, it is therefore, concluded that there are significant changes in the organoleptic parameters of the maize/ sweet potato corn jellos evaluated. The sensory Panelists preferred the appearance of the sweet potato substituted samples than the control sample which is 100% maize. There was no significant difference on the taste across all samples evaluated. The general acceptability were rated high by the sensory panelists across all samples except sample MSC5. The vitamin A content of the samples had a progressive increased as the OFSP inclusion increased with the control sample having least value. This making the product a good source of vitamin A thereby, complementing vitamin A from other sources for a weaning infant.

REFERENCES

1. Andreas, N. J., Kampmann, B., & Le-Doare, K. M. (2015). Human breast milk: A review on its composition and bioactivity. *Early human development*, *91*(11), 629-635.
2. AOAC.2012. Official methods of analysis (18th ed.). Gaithersburg, USA: AOAC International.
3. Cauvain, S. P.; Young, L. S. 2009. Bakery food manufacture and quality: water control and effects. John Wiley & Sons.
4. Faber, M., Laurie, S. M., & van Jaarsveld, P. J. (2013). Total β-carotene content of orange sweetpotato cultivated under optimal conditions and at a rural village. *African Journal of Biotechnology*, *12* (25).
5. Faber M, Laurie SM (2011). A home-gardening approach developed in South Africa to address vitamin A deficiency. In: Thompson B, Amoroso L, eds. combating micronutrient deficiencies: Food-based approaches. CABI and FAO, Rome. pp. 163-182.
6. FAO/WHO (1998). Preparation and use of Food-Based Dietary Guidelines. Report of a Joint FAO/WHO Consultation. WHO Technical Report series 880. Geneva. 15.
7. Francis, K.A, Jane, O.2014. Orange-fleshed sweet potato-based infant food is a better source of dietary vitamin A than a maize– legume blend as complementary food. Fd and Nutr. Bulletin, Vol. 35, No. 1.The *Nevin Scrimshaw International Nutrition Foundation*.
8. Haskell MJ, Jamil KM, Hassan F, Peerson JM, Hossain MI, Fuchs GJ, Brown KH (2004). Daily consumption of Indian spinach (Basella alba) or sweet potatoes has a positive effect on total-body vitamin A stores in Bangladeshi men. Am. J. Clin. Nutr. 80:705-714.
9. Hennet, T., & Borsig, L. (2016). Breastfed at Tiffany's. *Trends in Biochemical Sciences*, *41*(6), 508-518.
10. Idolo, I. 2011. Sensory and nutritional quality of Madiga produced from composite flour of wheat and sweet potato. Pakis J. of Nutri. *10*(11), 1004-1007.
11. Iwe, M.O. (2002). Handbook of sensory methods and analysis. Rojoint Com. Services Ltd., Enugu, Nigeria.
12. Korese, J. K. ;Chikpah, S. K. ; Hensel, O. ; Pawelzik, E. ; Sturm, B. 2021. Effect of orange-fleshed sweet potato flour particle size and degree of wheat flour substitution on physical, nutritional, textural and sensory properties of cookies. Eurp. Fd. Res. and Tech. *247*(4), 889-905
13. Kumar, D.; Jhariya, N.A.2013. Nutritional, medicinal and economic importance of corn: A mini review. Res J. of Pharm. Sc... 2: 7–8
14. Nwanagba, N. L. I. ; Obetta, A. N. ; Isaac, U. R. ; Nwachukwu, A. N. 2021. Evaluation of the Chemical Composition and Sensory Properties of Soy-agidi Fortified with Alternanthera brasiliana Powder. Nig. Agric. J. *52*(2), 400-407

15. Okwu, D. E.; Josiah, C. 2006. Evaluation of the chemical composition of two Nigerian medicinal plants. Afr. J. of Biotech. *5*(4), 357-361.
16. Olori-Great, N. G.; Okpara, D. A. 2021. Effect of Planting Date on Growth, Carotene and Root Yield of three Sweet potato Varieties [Ipomoea batatas (L.) Lam.] in South-East Nigeria. Nig. Agric. J. *52* (1), 221-228.
17. Onwuka, G., and Onwuka, N. (2005). The effects of ripening on the functional properties of plantain and plantain based cake, *International Journal of Food Properties 8* (2): 347-353.
18. Tadesse, T. F.; Nigusse, G.; Kurabachew, H. 2015. Nutritional, microbial and sensory properties of flat-bread (kitta) prepared from blends of maize (Zea mays L.) and orange-fleshed sweet potato (Ipomoea batatas L.) flours. Int. J. of Fd. Sci. and Nutri. Engr. *5* (1), 33-39.
19. Sant'Anna, G. M., & Keszler, M. (2012). Weaning infants from mechanical ventilation. *Clinics in perinatology*, *39* (3), 543-562.
20. World Health Organization. 2016. *WHO guideline:* use of multiple micronutrient powders for point-of-use fortification of foods consumed by infants and young children aged 6–23 months and children aged 2–12 years. World Health Organization.
21. Wu, F.; Xu, X. 2019. Sprouted Grains-based Fermented Products. In *Sprouted grains* (pp. 143-173). AACC International Press.

Electrochemical Study for using Eg-dronate drug as a Green Corrosion Inhibitor in 0.5 M H_2SO_4 Solution by Applied: Potentiodynamic and Evans Techniques

Adel H. Ali

Taiz University

ABSTRACT

In this paper using the Egy-dronate pharmaceutical drug compound as a green corrosion inhibitor that can decreasing the rate of corrosion on metallic surface, as a result of the adsorption of Egy-dronate on the metal surface. In this regard, we simultaneously present an overview of Egy-dronate compound performance, as a corrosion inhibitor in 0.5 M H_2SO_4, and with presence different concentrations of the drug. By using potentiodynamic polarization, and Evans techniques illustrate the nature of adsorption, the effect of medium on the corrosion processes, and the effect of polarization for the orientation of the inhibitor molecule to the CS surface. The surface examination by Scanning Electron Microscopy (SEM), Energy Dispersive X-ray (EDX), Atomic Force Microscopy (AFM), and Fourier Transforms Infrared (FT-IR) are confirmed the formation thin film that adsorbed on the metal surface according to the mechanism of the adsorption processes on the polarized metal surface.

Keywords: corrosion inhibition; potentiodynamic polarization; evans technique; egy-dronate inhibitor; SEM; EDX; AFM; FT-IR.

Classification: DDC Code: 541.33 LCC Code: QD547

Language: English

London Journals Press

LJP Copyright ID: 925624
Print ISSN: 2631-8490
Online ISSN: 2631-8504

London Journal of Research in Science: Natural and Formal

Volume 23 | Issue 3 | Compilation 1.0

Electrochemical Study for using Eg-dronate drug as a Green Corrosion Inhibitor in 0.5 M H_2SO_4 Solution by Applied: Potentiodynamic and Evans Techniques

Adel H. Ali

ABSTRACT

In this paper using the Egy-dronate pharmaceutical drug compound as a green corrosion inhibitor that can decreasing the rate of corrosion on metallic surface, as a result of the adsorption of Egy-dronate on the metal surface. In this regard, we simultaneously present an overview of Egy-dronate compound performance, as a corrosion inhibitor in 0.5 M H_2SO_4, and with presence different concentrations of the drug. By using potentiodynamic polarization, and Evans techniques illustrate the nature of adsorption, the effect of medium on the corrosion processes, and the effect of polarization for the orientation of the inhibitor molecule to the CS surface. The surface examination by Scanning Electron Microscopy (SEM), Energy Dispersive X-ray (EDX), Atomic Force Microscopy (AFM), and Fourier Transforms Infrared (FT-IR) are confirmed the formation thin film that adsorbed on the metal surface according to the mechanism of the adsorption processes on the polarized metal surface.

Keywords: corrosion inhibition; potentiodynamic polarization; evans technique; egy-dronate inhibitor; SEM; EDX; AFM; FT-IR.

Author: Department of Physics, Faculty of Science brunch of Al-Tourba, Taiz University, Yemen.

I. INTRODUCTION

Most organic compounds containing nitrogen (N-heterocyclic), sulfur, long carbon chain, or aromatic, and oxygen atoms are used as a corrosion inhibitors. Among them, organic compounds have many advantages such as large molecular size, soluble in water, availability, cheap, low toxicity, easy for using, and easy production [1]. Natural heterocyclic mixes have been utilized for the corrosion inhibitor on the C-steel [2], copper [3], aluminum [4], and various metals in various aqueous medium [5]. Adsorption of the drug molecules on the metal surface facilitates its inhibition [6]. Heterocyclic mixes have demonstrated more hindrance effectiveness, for C-steel in both HCl [7] and H_2SO_4 arrangements [8], such as the medications are used inhibitors, that can compete favorably with green inhibition of corrosion, and the most medications can be synthesized from natural products. Selection of some medication as corrosion inhibitors due to the followings: (1) drug molecules contain oxygen, sulfur, and nitrogen as active sites, (2) it is environmentally friendly furthermore vital in organic responses, (3) drugs can be easily produced, and purified, (4) nontoxic compering organic inhibitors. Some medications have been investigated to be great corrosion inhibitors for metals such as Biopolymer gave 86% inhibition efficiency (IE) for Cu in NaCl [9], pyromellitic diimide linked to oxadiazole cycle gave 84.6% IE for mild steel (MS) in HCl [10], 2-mercaptobenzimidazole gave 82% IE for MS in HCl Antidiabetic Drug Janumet gave 88.7% IE for MS in HCl [11]. Januvia gave 79.5 % IE for Zn in HCl [12],Cefuroxime Axetil gave 89.9% IE for Al in HCl [13], Phenytoin sodium gave 79% for MS in HCl [14], Aspirin gave71% IE for MS in H_2SO_4 [15], Septazole gave 84.8% IE for Cu in HCl [16] and

Chloroquine diphosphate gave 80% IE for MS in HCl [17]. Study on Structural, Corrosion, and Sensitization Behavior of Ultrafine and Coarse Grain 316 Stainless Steel Processed by Multiaxial Forging and Heat Treatment [18]. Investigating the corrosion of the Heat-Affected Zones (HAZs) of API-X70 pipeline steels in aerated carbonate solution by electrochemical methods [19]. Predictions of corrosion current density and potential by using chemical composition, and corrosion cell characteristics in microalloyed pipeline steels [20]. Predictions of toughness, and hardness by using chemical composition, and tensile properties in microalloyed line pipe steels [21].

The scope of this article is used Egy-dronate drug as save corrosion inhibitor for CS in the acid medium by electrochemical method, and to elucidate the mechanism of corrosion inhibition.

II. EXPERIMENTAL

2.1 Metal samples

The sample of CS was used in this study that have the chemical composition of the metal sample was determined by using an emission spectrometer, with the aid of ARL quant meter (model 3100-292 IC) and listed in the Table 1.

Table 1: Chemical compositions of carbon steel sample

Sample	C%	Mn%	V%	Fe%	Si%
CS	0.26	0.77	0.11	98.51	0.35

2.2 Preparation of metal sample (working electrode)

Working electrode having the surface area, which, exposed to corrosion media is (1Cm^2) cross-section area, and the rod was weld from one side to a copper wire used for electric connection. The sample was embedded in a glass of just a larger diameter than the sample. Epoxy resin was used to stick the sample to glass tube. These also ensured that a constant cross-sectional area would be exposed to corrosive media, through the experiments. The sample was scraped with SiC polisher sheet coarseness sizes (400, 800, and 1200), and clean with (CH3)2CO. Then, clean a few times with bi-distilled water, and dried by soft tissue. Finally, the polishing of sample surface become like a mirror bright, just before immersion in the electrolyte cell.

2.3 Egy-dronate drug as an inhibitor

Egy - dronate drug is mixed inhibitors which consists of two substances Alendronic acid, and Cholecalciferol which describing in Table 2.

Table 2: The Components and molecular structure of investigated inhibitor

Inhibitor	Structure		IUPAC Name	Molecular weight	Active centers	Chemical formula
(1)	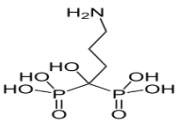 Alendronic acid	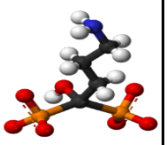	sodium [4-amino-1-hydroxy-1-(hydroxy-oxido-phosphoryl)-butyl]phosphonic acid trihydrate	249.097 g/mol	N 7O 2π	$C_4H_{13}NOP_2$

(2)	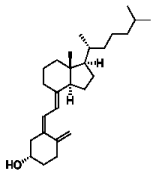 Cholecalciferol (Vit. D_3)	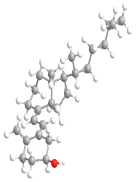	(3β,5Z,7E)-9,10-secocholesta-5,7,10(19)-trien-3-ol	384.64 g/mol	O 2π	$C_{27}H_{44}O$

2.4 Solution

The aggressive solution, 0.5 M H_2SO_4 was prepared by dilution of analytical grade (98 %) H_2SO_4 with bi-distill water. The concentrations range of the inhibitor were used between 50 ppm to 250 ppm.

2.5 Potentiodynamic polarization measurement

Cathodic, and anodic polarization technique were used for determination the rate of corrosion, by using the electrochemical cell that consists of three electrodes [22]:

1- A platinum electrode (as an auxiliary electrode).
2- Calomel electrode (as the reference electrode). ($Hg_{(l)}$ | $Hg_2Cl_{2(s)}$, $KCl_{(aq)}$sat,), E equal - 241 mV at 25°C.
3- The working electrode is the CS sample. The electrolytic cell was filled with 100 ml of the solution, and the sample was immersed in the medium. Then, the cathodic polarization was firstly measured, and after reverse the current direction the anodic polarization was measured.

2.6 Calculation of the rate of corrosion

The anodic, and cathodic polarization were measured by using the over-potential cells. The corrosion current density (I_{corr}), the corrosion potential (E_{corr}), and the corrosion rates (R) are calculated according to the Tafel extrapolation method [23].

It is clear that the line representing Tafel region refer by either cathodic, and anodic polarization curve, to obtain the corrosion potential (E_{corr}), and corrosion current density (I_{corr}), which can be used to calculate the rate of corrosion by the equation (1) [24-25].

$$\text{Corrosion rate (mpy)} = 0.1288\ I\ (\text{mA/cm2})\ \text{Eq.wt}\ /d\ (\text{g/cm3}) \quad (1)$$

Where, Corrosion rate (mpy) = mils per yea ,I = the corrosion current density, d = Specimen density, and, Eq.wt = Specimen equivalent weight.

The corrosion current density (I_{corr}), corrosion potential (E_{corr}), and corrosion rate are recorded in Table 5.

2.7 Applied Evans technique

The Evans diagrams give good and suitable interpretation of the electrode-electrolyte interface reactions. We can use the following definitions for the items of Evans diagram as follows [26]:

1- $\Delta\phi_{e,m}$ and $\Delta\phi_{e,so}$ are anodic and cathodic potentials at equilibrium at the electrode-electrolyte interface (at I =the exchange current i_o) respectively, where $\Delta\phi e,x = E_{e,x} \pm |E_c - E_a|\ i=i_o$; m= metal, so= solution,
2- $\Delta\phi = \Delta\phi_{corr}$ = the relative corrosion potential determined from the position of the intersection of the two curves (de-electronation and electronation processes) where I considered as the i_{corr}.

3- The anodic- potential difference at equilibrium (a.p.d,e) $\Delta\phi'_m = \eta_m = \Delta\phi_{corr} - \Delta\phi_{e,m}$.
4- The cathodic- potential difference at equilibrium (c.p.d,e) $\Delta\phi'_s = \eta_{so} = \Delta\phi_{corr} - \Delta\phi_{e,so}$.
5- The anodic-potential difference (a.p.d) $\Delta\phi'_a = (\Delta\phi_a)_x - (\Delta\phi)_b$; b =bulk, x = with additive, at different concentrations or at different temperatures, and $\Delta I_a = (i)_b - (I)_x$.
6- The cathodic-potential difference (c.p.d) $\Delta\phi'_c = (\Delta\phi)_b - (\Delta\phi_c)_x$; b=bulk, x= with additive, at different concentrations or at different temperatures, and $\Delta I_c = (i)_b - (I_c)_x$.

These data can be used for kinetic calculations, and to know, which additive is favorable, or which is faster to the electrode surface at the same conditions. It can be used for studying the inhibition mechanism.

2.8 Surface Examinations [27]

The morphology of the CS surface is used for the analysis by examination nature of the surface, and study of changing that appeared on the metal surface. The specimens were prepared by abraded mechanically by using different emery papers up to 1200 grit size, and immersed in 0.5 M H_2SO_4 (blank) then with 250 ppm of Egy-dronate at room temperature for one day (24 h). Then, after that the specimen was washed gently with distilled water, dried carefully, and take care to the system of surface examinations by Fourier Transforms infrared (FT-IR), scanning electron microscope (SEM), energy dispersive x-ray (EDX), and atomic force microscope (AFM).

III. RESULT AND DISCUSSION

3.1 Potentiodynamic polarization technique

Study the polarization of the different medium, and with added the various concentrations of Egy-dronate as a corrosion inhibitor.

3.1.1 Dissolution of CS sample in 0.5N H_2SO_4 at different temperatures

Results of the anodic, and cathodic polarization processes for the CS sample in 0.5M H_2SO_4 at different temperatures in the absence of Egy-dronate are shown in **Figure 1**, and **Table 5**. It was obvious that the corrosion current density (I_{corr}) is increased as the temperature increased, and the corrosion potential (E_{corr}) is slightly shafted to the more positive value. The polarization processes are started with a potential between about 547, and 553 mV.

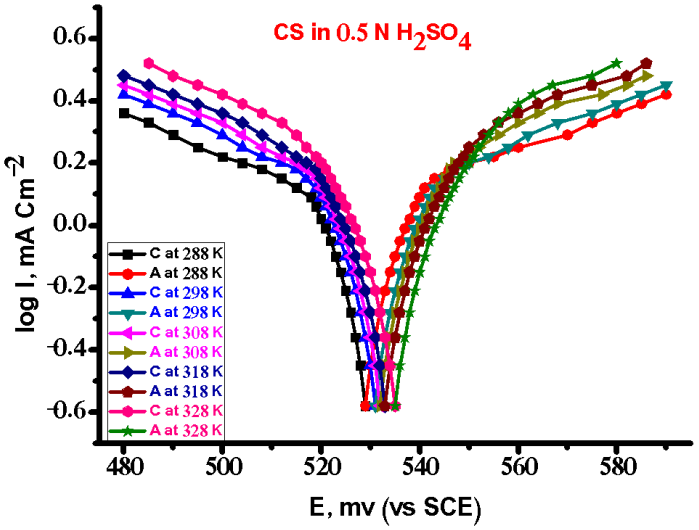

Figure 1: The potentiodynamic polarization curves for corrosion of CS in 0.5 M of H_2SO_4

The positive potential is increased by anodic polarization, i.e., increase the dissolved component while that the potential decreased by cathodic polarization, i.e., increase the undissolved components. The dissolved component is formed as the following chemical equations [28]:

$$Fe \rightarrow Fe^{2+} + 2e$$
$$Fe^{2+} + 2H_2O \rightarrow HFeO^-_2 + 3H^+$$

Where $HFeO^-_2$ Di-hypo-ferrite, green.

In the same time occurs as

$$HFeO_2^- + H^+ \rightarrow Fe(OH)_2$$

Where the undissolved hydrated, and the (FeO) can be considered. So that at anodic polarization in the presence of H_2SO_4, the iron is dissolved, and formed ferrous sulfate as:

$$Fe^{2+} + H_2SO_{4(aq)} \rightarrow Fe\,SO_{4(aq)} + 2H^+$$

And the cathodic processes in the presence of H_2SO_4 occurred as

i) $2H^+ + 2e \rightarrow H_2$ hydrogen evolution

ii) $O_{2(g)} + 4H^+_{(aq)} + 4e \rightarrow 2H_2O_{(l)}$ reduced of oxygen

The hydrogen ions adsorbed on the metal surface where an electrochemical reaction takes place in the presence of O_2 as:

$$M + H_3O^+ + e \rightarrow M{-}H + H_2O$$

Where three steps can be done as:

a. $2M{-}H \rightarrow 2M + H_{2(g)}\uparrow$
b. $M{-}H + H_3O^+ + e \rightarrow M + H_{2(g)}\uparrow + H_2O$ or
c. $4M{-}H^+ +$ dissolved $O_2 + 4e \rightarrow 4M + 2H_2O_{(l)}$

The positive potential is increased by anodic polarization, i.e. increase the dissolved component while that the potential decreased by cathodic polarization, i.e., increase the undissolved components. According to the following equation:

$$Fe \rightarrow Fe^{2+} + 2e \qquad \text{anodic reaction}$$

$$2H_2O + 2e \rightarrow H_{2\,(g)} \uparrow + 2OH^- \qquad \text{cathodic reaction}$$

In total process:

$$Fe + H_2O \rightarrow Fe^{2+} + 2OH^- \rightarrow Fe(OH)_2$$

In the bulk the ferrous hydroxide dissolved as:

$$2Fe(OH)_2 \rightarrow 2FeOH^{++} + 2OH^-$$

And,

$$2Fe\,OH^{++} + 2e \rightarrow 2Fe\,O + H_2\uparrow$$

3.1.2 Effect of add different concentration of Egy-dronate inhibitor

The anodic, and cathodic polarization of the CS in a mixed solution 0.5 M H_2SO_4 with different concentrations of the Egy-dronate (50, 100, 150, 200, and 250 ppm) at 288K are shown in the Figure 2.

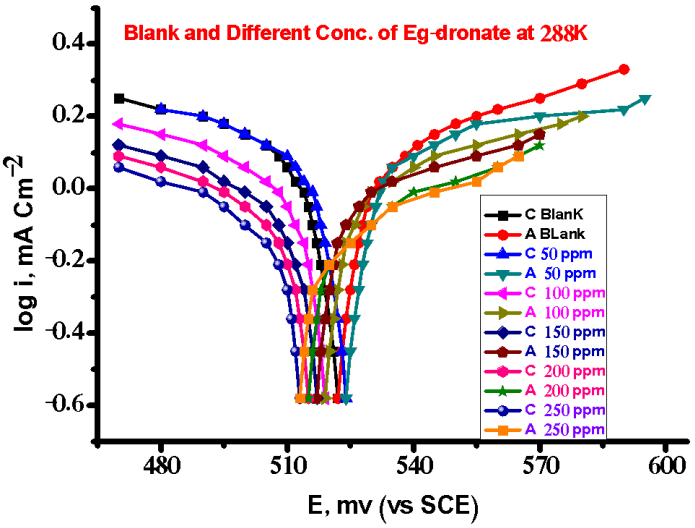

Figure 2: The potentiodynamic polarization curves for the corrosion of the CS in 0.5 M H_2SO_4 with the existence various concentration of the Egy-dronate at 288K.

3.13 Potentiodynamic polarization technique

It is obvious that the presence of different concentrations are shifted the potentials to low positive values, both anodic potential E_a, and cathodic potential E_c are shifted to low positive values [29]. The anodic current (i_a) slightly decreased (shifted to low values) while the cathodic (i_c) decreased, and shifted to low values too, that are shown in Figure 3. The values of the corrosion potential (E_{corr}), the corrosion current density (I_{corr}), and the rate of corrosion in (mpy) are given in Table 5.

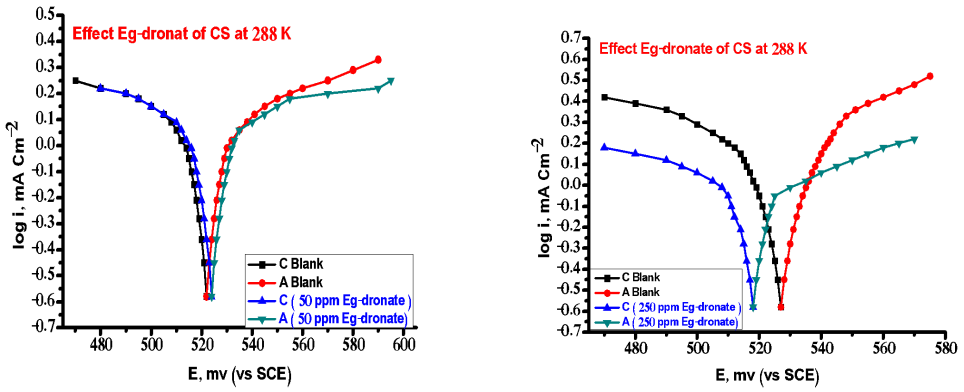

Figure 3: Effect of added the various concentrations of Egy-dronate for anodic, and cathodic polarization curves of the CS metal at 288K**.**

2 Applying Evans technique

Applying the principle of Evans diagrams in the presence of different concentrations from the Egy-dronate, which are viewed in Figures 4, and the Evans diagram parameters are listed in Table 3, it is clear that[30]:

The parameters ($\Delta\phi_{corr}$), (i_{corr}), ($\Delta\phi'_m$), (α_a), ($\Delta\phi'_a/\Delta I_a$), and ($\Delta\phi'_c/\Delta I_c$) are decreased with increasing the temperatures. In the other hand the ($\Delta\phi'_s$), (α_c), $|\Delta\phi'_a|$,$|\Delta\phi'_c|$, $|\Delta I_a|$, and $|\Delta I_c|$ are increased with the temperatures increased.

From the above results that are illustrated by Evans diagrams for the electrode- electrolyte interface of the CS. It is clear that:

In the presence various concentrations of the Egy-dronate under polarization technique. At low Egy-dronate concentrations the de-electronation potential shifted toward more positive values (positive direction), this means that the polarization are affected the donor functional groups of the Egy-dronate molecules, oriented them to the electron sink area on the electrode surface, and slow done the dissolution of the metal. The size of the Egy-dronate molecules allow to cover somewhat area of electron source, so that the electronation potential of acceptor spices shifted to low positive value. It is observed that the shifted of the de-electronation potential is larger than the shifted of the electronation potential. In the other hand the Egy-dronate concentrations increasing the shift of the electronation potential i.e., the Egy-dronate molecules are covered more electron source area on the corroded metal surface with increasing Egy-dronate concentrations, and the electronation potential shift is being that the larger than the de-electronation potential shift, which indicating that the slightly formation of multilayer, which adsorbed on the metal surface. It is clear that the polarization process affects the orientation, and the adsorption of the inhibitor molecules, so that both the metal dissolution, and the hydrogen evolution are slowing down more.

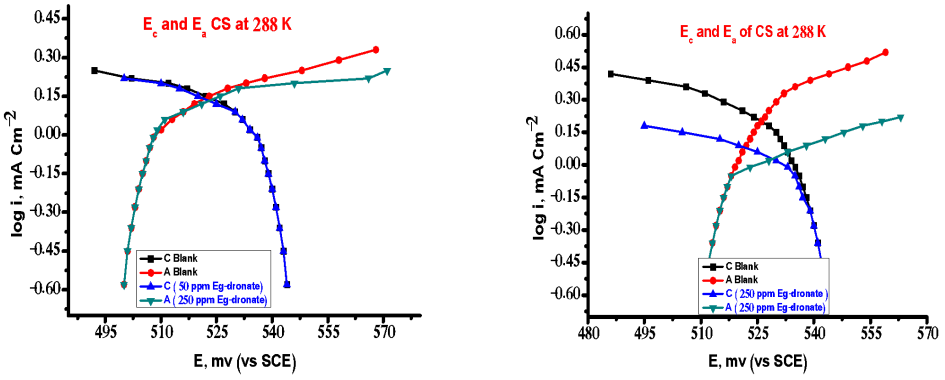

Figures 4: Evans diagrams of the electronation, and the de-electronation potentials vs. log I for CS with various concentrations of the Egy-dronate at 288K.

Table 3: Relative parameters from Evans diagram of CS with various concentrations of the Egy-dronate at 288K.

Conc. ppm	Δφcorr	Icorr	Δφe,m	Δφe,so	Δφ'm	Δφ's	(i)b	(Δφ)b	(Δφ'a)x	Δφ'a	(ΔIa)x	ΔIa*	Δφ/ΔI,a	(Δφ'c)x	Δφ'c	(ΔIc)x	ΔIc	Δφ'/ΔI,c	α,a	α,c
50	527	1.3	498	546	28	22	1.54	524	529	5.1	1.4	0.11	49.5	521	2.1	1.4	0.04	57.24	0.57	0.45
250	520	1.1	498	546	22	26	1.54	524	537	13.1	1.12	0.41	31.2	511	13.3	1.17	0.35	38.45	0.49	0.51

3.1.4 Effect of temperature on corrosion behavior

The results of the anodic, and cathodic polarization processes for the CS sample in the corrosive medium are listed in Table 5. The E_{corr}, I_{corr}, and the rate of corrosion were increased with the temperatures increased at the same concentration 150 ppm of Egy-dronate Figure 5.

1. Potentiodynamic polarization technique

The behavior of the anodic, and cathodic polarization are indicated that the rate of corrosion of the CS are stimulated by increasing of the temperature. The increasing of temperatures will be enhance the rate of diffusion of hydrogen (H^+) ion to the metal surface beside the ionic mobility, and increasing the conductivity of the electrolyte. Also, at lower temperatures, absorbed hydrogen atoms which are blocked on the cathodic areas, otherwise the increasing the temperatures of the solution, hydrogen will be disrobed from the cathodic area, i.e., the corrosion rate was increased.

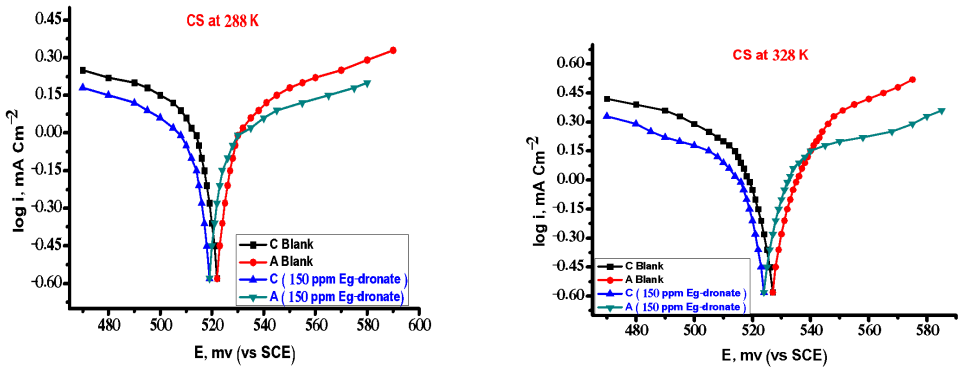

Figure 5: Effect of the temperatures in the presence 150 ppm of the Egy-dronate on anodic, and cathodic polarization curves of the CS metal.

1- Apply Evans technique

From the Evans diagrams in the presence of 150 ppm Egy-dronate, which are viewed in Figure 6, and the Evans diagram parameters are listed in Table 4, it is clear that:

The parameters ($\Delta\phi_{corr}$), ($\Delta\phi'_m$), (α_a), | $\Delta\phi'_c$ |, ($\Delta\phi'_a/\Delta I_a$), and ($\Delta\phi'_c/\Delta I_c$) are decreased with increasing the temperatures. In the other hand (i_{corr}), ($\Delta\phi'_s$), (α_c), | $\Delta\phi'_a$ |, $|\Delta I_a|$, and $|\Delta I_c|$ are increased with increasing the temperatures.

From the results that illustrated in Evans diagrams for the electrode-electrolyte interface it is clear that:

The effect of the temperature on the behavior of the Egy-dronate as an inhibitor of the CS corrosion at 150 ppm is discussed. It is obvious that both the electronation, and the de-electronation potentials are shifted to negative, and positive direction respectively by increasing the temperature. This behavior clarify that the metal surface divided the electron sink, and electron source area to the small parts, so that the size of the Egy-dronate sufficient to cover more electron source area be side electron sink.

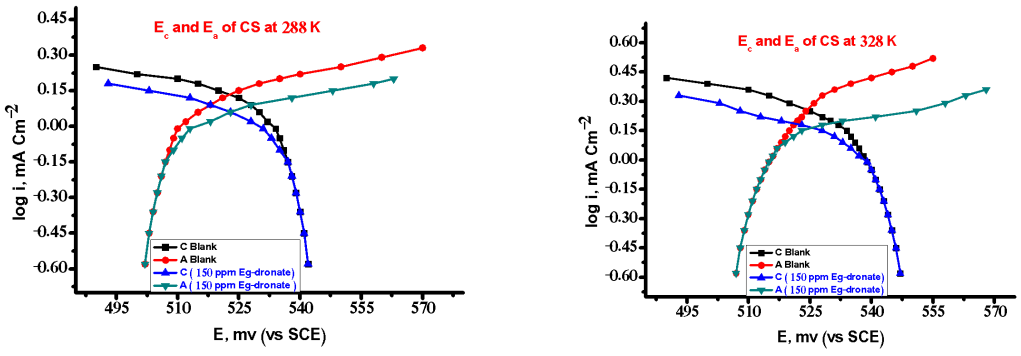

Figure 6: Evans diagrams of the electronation and the de-electronation potentials vs. log I for CS in the presence of 150 ppm of the Egy-dronate at various temperatures.

Table 4: Relative parameters from Evans diagram of CS in presence of 150 ppm of Egy-dronate at various temperatures.

Temp.	Δϕcorr	Icorr	Δϕe,m	Δϕe,so	Δϕ'm	Δϕ's	(i)b	(Δϕ)b	(Δϕ'a)x	Δϕ'a	(ΔIa)x	ΔIa*	Δϕ/ΔI,a	(Δϕ'c)x	Δϕ'c	(ΔIc)x	ΔIc	Δϕ'/ΔI,c	α,a	α,c
288	520	1.17	502	546	29	17	1.43	527	531	3	1.2	0.21	12.89	519	11	1.2	0.1	80	0.6	0.4
328	529	1.6	495	556	30	31.1	2.21	522	538	15.1	1.75	0.61	27.22	510	6.1	1.9	0.41	15	0.49	0.5

Table 5: The effect of Egy-dronate additions on the E_{corr}, I_{corr} and rate of corrosion for CS in 0.5 H_2SO_4 at various temperatures

Conc. (ppm)	Temp. K	Ecorr (mV)	Icorr (mA/Cm2)	Rate (mpy)	Θ	% IE
0	288	541	11.5	4.89	----	----
	298	542	11.7	4.98	----	----
	308	543	12.1	5.16	----	----
	318	544	12.7	5.41	----	----
	328	546	13.4	5.71	----	----
50	288	540	2.45	1.04	0.787	78.7
	298	541	2.49	1.06	0.787	78.7
	308	542	2.55	1.09	0.789	78.9
	318	544	2.62	1.12	0.793	79.3
	328	546	2.74	1.17	0.796	79.6
100	288	538	2.41	1.03	0.791	79.1
	298	539	2.45	1.04	0.791	79.1
	308	540	2.53	1.08	0.791	79.1
	318	541	2.58	1.10	0.797	79.7
	328	542	2.68	1.14	0.800	80.0
150	288	536	2.38	1.01	0.793	79.3
	298	537	2.42	1.03	0.793	79.3
	308	538	2.49	1.06	0.794	79.4
	318	539	2.55	1.09	0.799	79.9
	328	540	2.60	1.12	0.806	80.6
200	288	534	2.35	0.99	0.796	79.6
	298	535	2.39	1.02	0.795	79.5
	308	536	2.46	1.05	0.797	79.7
	318	537	2.51	1.07	0.802	80.2
	328	538	2.56	1.09	0.809	80.9
250	288	532	2.33	0.99	0.797	79.7
	298	533	2.36	1.01	0.798	79.8
	308	534	2.41	1.03	0.801	80.1
	318	535	2.47	1.05	0.806	80.6
	328	536	2.54	1.08	0.810	81.0

3.2 Inhibition efficiency (IE %)

The Egy-dronate compound possess eight active centers like nitrogen, oxygen atoms, and π-bonding are acted as a donor centers. As a result of the restricted un-plainer structure of the Egy-dronate, and some active sites are acted as a donor centers. These centers are oriented, and adsorbed on anodic sites (iron carbide), due to the Egy-dronate molecule is attached to the anodic site, and covered somewhat of cathodic area, so that the corrosion rate in the presence of Egy-dronate is regarded anodic-cathodic control. The inhibition efficiency (IE %) is calculated as following [31].

$$IE\ \% = [(I_{corr} - I'_{corr})/I_{corr}] \times 100 \quad (1)$$

Where I_{corr}, and I_{corr}' are the corrosion current densities in the absence, and the presence of an inhibitor respectively. The inhibition efficiency data is listed in Table7. It is obvious that the IE % for the CS sample increases with increasing the Egy-dronate concentrations.

Plot IE % against logarithm of the concentrations of Egy-dronate inhibitor (log [In]). It is obvious that the increases of the IE % with the temperatures of the medium are increased, this behavior is indicated that chemisorption's occurs. See Figure 7. The extra part in the curvatures that obtained from polarization technique like *f* shape indicating that the multilayer proceed from the orientation of functional group under polarization where causes second chemical adsorption over the first layer [32].

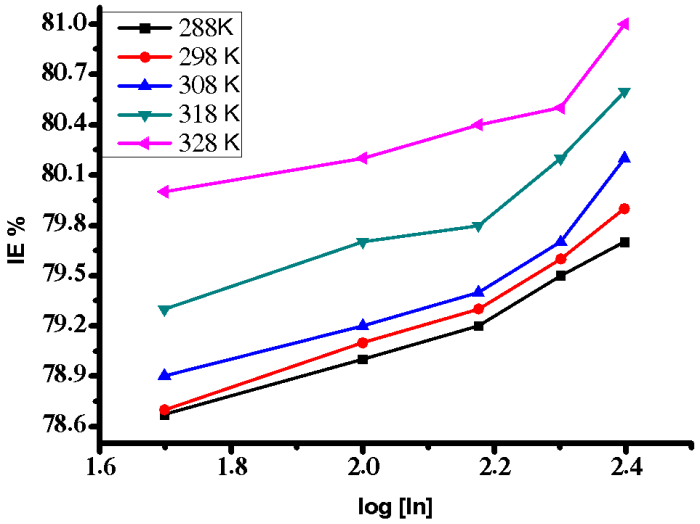

Figure 7: The relation between the IE %, and log [In] in 0.5 M H_2SO_4 for CS at various temperatures.

3.3 Scanning Electron Microscopy (SEM)

The micrographs are obtained for CS specimens in the nonexistence, and in the existence of 250 ppm of Egy-dronate drug after exposure for immersion one day in corrosive medium 0.5 M H_2SO_4. It is clear that CS has suitable surfaces for corrosion attack in the blank or corrosive medium only Figures 8 a, b and c. When the Egy-dronate is existence in the corrosive medium, the morphology of CS surfaces is quite different from the previous one, and the specimen surface was smoother. It is clear that the formation of a thin film layer adsorbed on the metal surface, which distributed in a disorder way overall

surface of the CS [33]. This may be due to the adsorption of the Egy-dronate on the CS surface, and made up the passive film in order to block the active site present on the CS surface. The Egy-dronate molecule is interacted with active sites of CS surface, resulting the decreasing contact between CS, and the corrosive medium. From the above sequentially Egy-dronate is exhibited excellent inhibition effect.

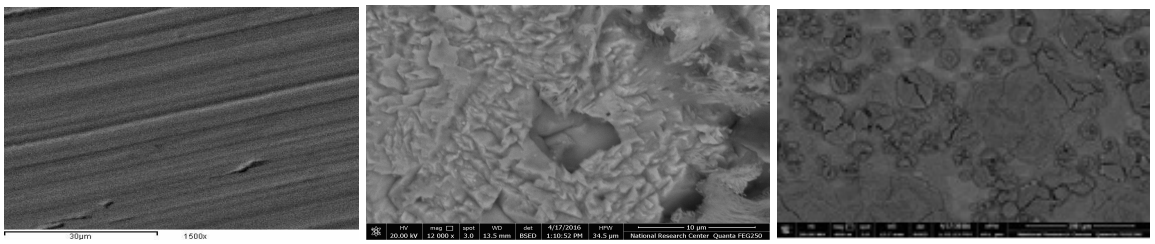

a-Free sample (LCH) b- Blank in 0.5M H_2SO_4 c-In 0.5 M H_2SO_4 with existence 250 ppm of Egy-dronate

Figures 8 a, b and c: SEM micrographs for CS in the nonexistence, and the existence of 250 ppm of the Egy-dronate after submersion for 1 day

3.4 Energy Dispersion Spectroscopy (EDX) [34]

To determination the elements, and molecules that existence are adsorbed on the surface of CS after one day that immersion in acid with optimum doses of Egy-dronate by using the EDX spectra. The EDX analysis of CS in 0.5 M H_2SO_4 with in the presence of 250 ppm of the Egy-dronate is given by **Figure 9**. The spectra show additional lines, demonstrating the existence of C (owing to the carbon atoms of some Egy-dronate). These data shows that the carbon, nitrogen, and oxygen atoms are covered the specimen surface. The EDX analysis is indicated that only carbon, nitrogen, and oxygen are detected, and show that the passivation film is contained the chemical formula of the Egy-dronate drag that adsorbed on the CS surface. It is clear that, the percent weight of adsorbed elements C, N, and O were presented in the spectra, and recorded in Table 6.

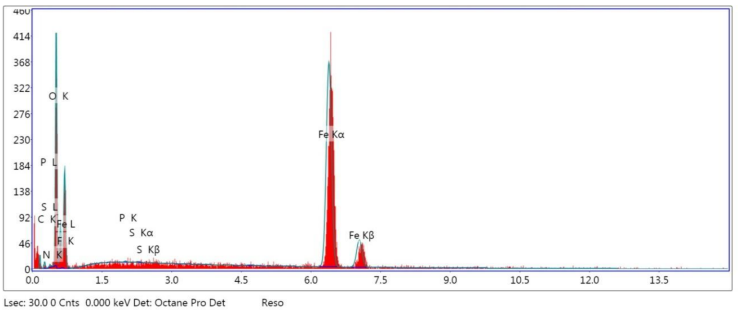

Figure 9: EDS analysis on the CS in the existence 10 x 10^{-5}M of the Egy-dronate drug for 1 day that immersion in 0.5 M H_2SO_4.

Table 6: Surface composition (wt %) of CS after one day that immersion in 0.5 M H_2SO_4 with 250 ppm of the Egy-dronate

Wt %	Fe	C	N	O
Egy - dronate	75.97	2.08	1.88	20.68

3. 5 Atomic Force Microscopy (AFM)

AFM is a powerful tool to investigate the surface morphology of various samples at nano- micro scale that is currently used to study the influence of corrosion inhibitor on the metal solution interface. From the analysis, it can be gained regarding the roughness on the surface. The roughness profile values is played an important role to identifying, and report the efficiency of the inhibitor under study. Among the roughness is tacked a role for the explanation of adsorption, and illustrated the nature of the adsorbed film on the metal surface [35-36]. Figure 10 a, shows the 3D images as well as elevation profiles of polished of the CS in the absence, and the presence the Egy-dronate as an inhibitor. Figure 10 b, the surface of CS specimen (a) exposed to corroded solution affected vales structure with large, and deep crack but the surface (b) reveal that is covering film adsorbed on the metal surface. Conclusion, the adsorption film is protected the surface of the metal from corrosion process. From analysis the values, indicating that the higher value of Z parameter reached, which found (2.60 µm) for the blank solution which placed in 0.5 M H_2SO_4 one day and analyzed. The observation of the metal surface which immersed in 0.5 M H_2SO_4 in the presence of 10 x 10^{-5}M of the Egy-dronate as an inhibitor possess small roughness (259.14 nm) compared with the blank solution. It can be noted that the value is lower than that of the blank value. The decrease in the roughness value reflected to the adsorption of inhibitor molecule on metal surface thereby reducing the rate of corrosion.

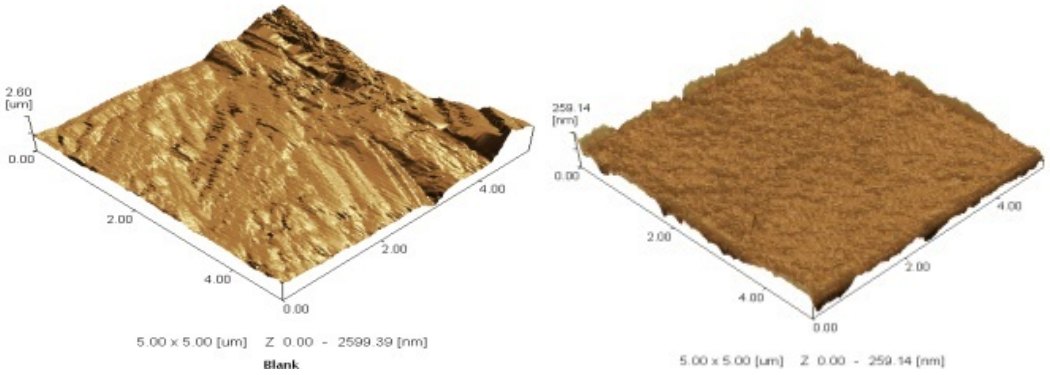

a-Blank b-In 250 ppm of Egy- dronate drug

Figure 10 a and b: The 3D of optical images of AFM in the nonexistence, and the existence of the Egy-dronate drug.

3.6 Fourier transforms infrared spectra (FT – IR)

The (FT – IR) spectrophotometer is a powerful instrument that can be used to identify the function group that presence in organic compounds and the type of interaction that occur between function group with metal surface. Since, pharmaceutical drug compound contain variety of organic compound, and these organic compounds (inhibitor) are adsorbed on the metal surface providing thin film that protection them against corrosion, they can be analyzed by using (FT – IR). To confirm the nature of the chemical constituent is adsorbed on the metal surface, by the Fourier transform infrared (FT – IR) spectra [37].

The pharmaceutical drug compounds are certain have function group according to the chemical formula like OH, C=C and P=O. In order to find the nature of constituents involved in the adsorption using (FT – IR) spectrum of material that are coated the metal surface gives in Figures 11. The spectrum of Egy – dronate before, and after adsorption that seen the wave number of the function groups OH abroad peak at 3400 cm^{-1} starching, C=C is sharp peak at 1630 cm^{-1} starching, and P=O a

sharp peak between 1140 – 1000 cm^{-1} starching. It is clear that the function groups of Egy – dronate inhibitor appear on the metal surface that confirm to the adsorption process [38].

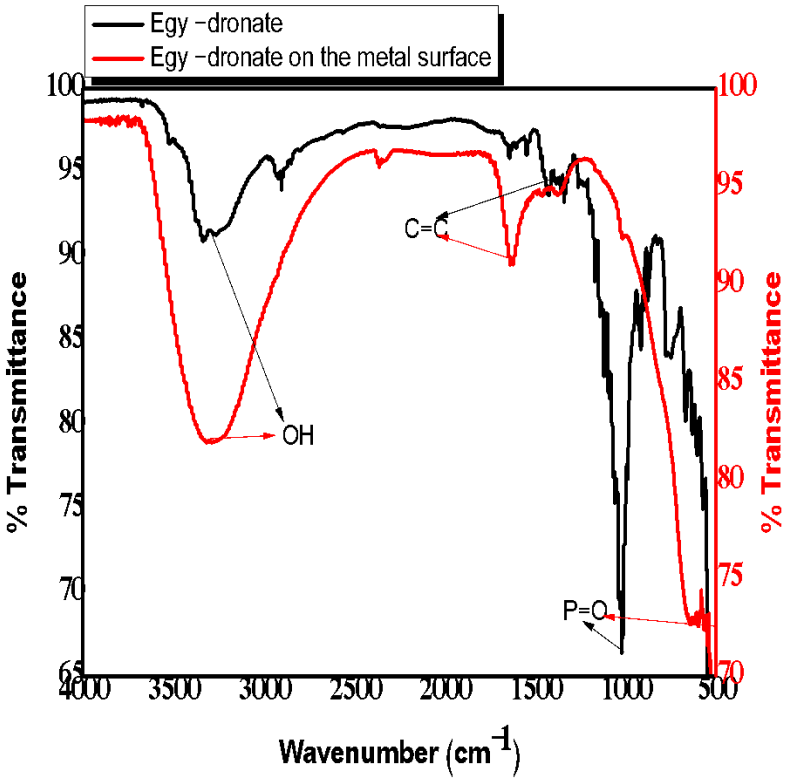

Figure 11: FT – IR spectrum of Egy - dronate before and after adsorption on the CS surface.

3.7 Mechanism of inhibition

To illustrate the mechanism of inhibition of corrosion on the CS surface in acid medium by using pharmaceutical drug compound as an inhibitor, it is must be know the nature of metal surface, and the nature of the component of inhibitor structure. The CS is regarded the metal α-phase [39], It is obvious that α-phase state consists of grains, and grain boundaries in the surface of the metal, Figure 12. A cross-section of a piece or specimen of the metal that is a corroding to clarify that there are both anodic, and cathodic sites in the metal surface structure.

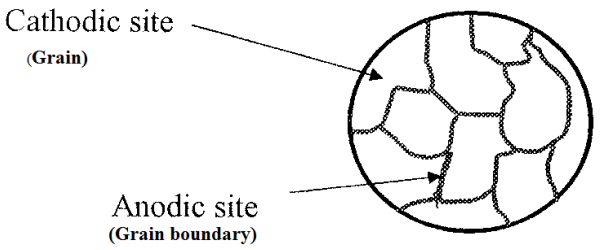

Figure 12: Schema models of metalα- phase

The surface of iron is usually, coated with a thin film of iron oxide. However, if this iron oxide film develops some cracks, anodic area are created on the surface, while other metal parts acts as cathodic sets. It follows that the anodic areas are small surface, while nearly the rest of the surface of the metal large cathodes. Electrochemical corrosion involves flow of electric current between the anodic, and

cathodic areas called inter-granular corrosion. Figure 13, SEM image is shown the corrosion of the CS in 0.5 N H_2SO_4in one day immersion that illustrated inter-granular corrosion.

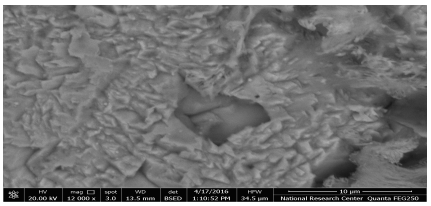

Figure 13: SEM image illustrated inter-granular corrosion after immersion the specimen in 0.5N H_2SO_4one day

All previous results prove that the pharmaceutical drug compound under study were actually inhibit the corrosion of the CS in 0.5 M H_2SO_4 solution as a corrosive medium. The corrosion inhibition is due to their physical, and chemical adsorption for formation of protection thin film adsorbed on the metal surface. The effect of Egy-dronate as inhibitor may be corresponding to the accumulation of the inhibitor molecules on the metal surface, which prevent the direction contact of the metal surface with corrosive environment. The surface of the CS sample have positively charge in aqueous acid solution, and the adsorption occur according to [40]:

1- The unshared electrons of nitrogen, oxygen atoms, and electron density of π bonding donate to the vacant orbital on the metal surface make chemisorption.
2- The partial negative charge that present in function group containing Oxygen, nitrogen, and electron density of π-bond in Egy-dronate may be adsorbed on the positively charge of the metal surface like electrostatic attraction between the opposite charge, in the form of neutral molecules, that involving displacement of water molecules from the metal surface.

The inhibition action of the Egy-dronate can be accounted by the interaction between the lone pair of electrons in the nitrogen, oxygen, and electron density of π-bond with positively charged (anodic sites) on the metal surface, and the skeleton of inhibitor compound cover the cathodic sites this action form thin layer adsorbed on the metal surface and prevent corrosion processes Figure 14.

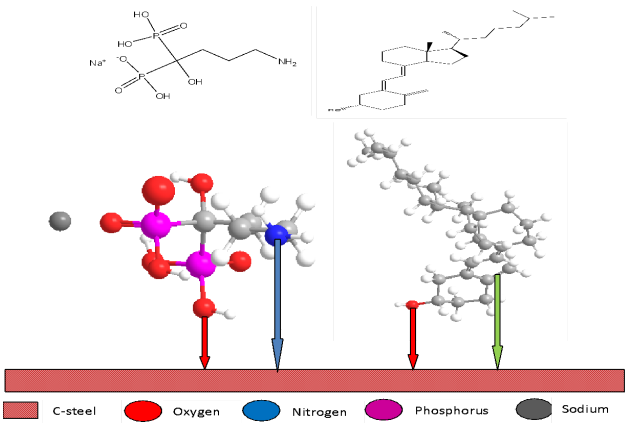

Figure 14: Schema model illustrated the adsorption of the Egy-dronate structure on the CS surface.

This meaning, the Egy-dronate molecule attached with anodic site, and covered somewhat of cathodic area, so that the corrosion rate in presence of Egy-dronate is anodic-cathodic control.

IV. CONCLUSION

Inhibition of the corrosion of the CS in 0.5 M H_2SO_4 solution by Egy-dronate is determine by potentiodynamic polarization, Evans techniques, and surface examination by Scanning Electron Microscopy (SEM), Energy Dispersive X-ray (EDX), Atomic Force Microscopy (AFM), and Fourier Transforms Infrared (FT-IR). It was found that the inhibition efficiency depends on concentration, nature of metal surface, and the type of adsorption of the inhibitor. The observed corrosion data in the presence the Egy-dronate as an inhibitor:

1) The tested Egy-dronate inhibitor establish a very good an inhibition efficiency for the CS corrosion in 0.5 M H_2SO_4 solution.
2) Egy-dronate inhibit the CS for the corrosion by the adsorption on its surface, and make thin film layer protective them from corrosion process.
3) The inhibition efficiencies of the Egy-dronate increases with the increasing of their concentrations.
4) The values of inhibition efficiencies obtained from all techniques that using are seen the validity of the obtained results.
5) The Egy-dronate molecule attached with anodic site, and covered somewhat of cathodic area, so that the corrosion rate in the presence of the Egy-dronate is anodic-cathodic control.

REFERENCES

1. Raspini I. A., (1993) Influence of Sodium Salts of Organic Acids as Additives on Localized Corrosion of Aluminum and Its Alloys, Corrosion, 49, 821-828.
2. Migahed M. A., Azzam E. M. S., Al-Sabagh A. M. , (2004) Corrosion inhibition of mild steel in 1 M sulfuric acid solution using anionic surfactant Mater. Chem. Phys., 85, 273-279.
3. Villamil R. F.V., Corio P., Rubim J. C., Siliva M. L., (1999) Effect of sodium dodecylsulfate on copper corrosion in sulfuric acid media in the absence and presence of benzotriazole, J. Electroanal. Chem., 472, 112-119.
4. Abd El Rehim S. S., Hassan H., Amin M. A. , (2003) The corrosion inhibition study of sodium dodecyl benzene sulphonate to aluminum and its alloys in 1.0 M HCl solution Mater. Chem. Phys., 78, 337-348.
5. Guo R., Liu T., Wei X., (2002) Effects of SDS and some alcohols on the inhibition efficiency of corrosion for nickel, Colloids Surf., A, 209, 37-45.
6. Branzoi V., Golgovici F., Branzoi F., (2002)Aluminum corrosion in hydrochloric acid solutions and the effect of some organic inhibitors, Mater. Chem. Phys., 78, 122-131.
7. Elachouri M., Hajji M. S., Salem M., Kertit S., Aride J., Coudert R., Essassi E., (1996) Some Nonionic Surfactants as Inhibitors of the Corrosion of Iron in Acid Chloride Solutions, Corrosion, 52,103-108.
8. Algaber A. S., El-Nemma E. M, Saleh M. M., (2004) Effect of octylphenol polyethylene oxide on the corrosion inhibition of steel in 0.5 M H_2SO_4, Mater. Chem. Phys., 86, 26-32.
9. Oukhrib R., El Ibrahimi B., Bourzi H., El Mouaden K., Jmiai A., . El Issami S, Bammou L., Bazzi L., (2017) Quantum chemical calculations and corrosion inhibition efficiency of biopolymer “chitosan” on copper surface in 3% NaCl, JMES, 8 (1), 195-208.
10. Al-Azzawi A. M., and Hammud K. K., (2016)Newly antibacterial / anti-rusting oxadiazoleporomellitic di-imids of carbon steel / hydrochloric acid interface: Temkin isother model, IJRPC, 6 (3), 391-402.
11. Umar M. Sani1 , Umar Usman, (2016) Electrochemical Corrosion Inhibition of Mild Steel in Hydrochloric Acid Medium Using the Antidiabetic Drug Janumet as Inhibitor, International Journal of Novel Research in Physics Chemistry & Mathematics, 3 (3), 30-37.
12. Kolo A. M., Sani U.M., Kutama U., and Usman U., (2016) The Pharmaceutical and Chemical Journal, 3 (1), 109-119.

13. Ameh P. O. and Sani U. M., (2015) Cefuroxime Axetil: A Commercially Available Pro-Drug as Corrosion Drug for Aluminum in Hydrochloric Acid Solution, Journal of Heterocyclic, 1(1), 2 – 6.
14. Al-Shafey H. I., Abdel Hameed R. S., Ali F. A., Aboul-Magd A. S., Salah M., (2014) Effect of Expired Drugs as Corrosion Drugs for carbon steel in 1M HCL Solution, Int. J. Pharm. Sci. Rev. Res. 27(1), 146-152.
15. Rupesh Kushwah, Pathak R. K., (2014) Inhibition of Mild Steel Corrosion in 0.5 M Sulphuric Acid Solution by Aspirin Drug, International Journal of Emerging Technology and Advanced Engineering, 4 (7), 880-884.
16. Fouda A. S., EL-Haddad M.N., and Abdallah Y. M., (2013) Septazole: Antibacterial Drug as a Green Corrosion Drug for Copper in Hydrochloric Acid Solutions, IJIRSET, 2 (12), 7073-7085.
17. Ofoegbu S. U. and Ofoegbu P. U., (2012) Corrosion inhibition of MS in 0.1 M hydrochloric acid media by chloroquine diphosphate , ARPN Journal of Engineering and Applied Sciences, 7 (3), 272-276.
18. Kiahosseini S. R., S. Baygi J. M., Khalaj G., Khoshakhlagh A., and Samadipour R., (2018) Study on Structural, Corrosion, and Sensitization Behavior of Ultrafine and Coarse Grain 316 Stainless Steel Processed by Multiaxial Forging and Heat Treatment, Journal of Materials Engineering and Performance, 27, 271–281.
19. Gholamreza K., Mohammad-Javad K., (2016) Investigating the corrosion of the Heat-Affected Zones (HAZs) of API-X70 pipeline steels in aerated carbonate solution by electrochemical methods, International Journal of Pressure Vessels and Piping, 145, 1-12.
20. Narimani N., Zarei B., Pouraliakbar H., Khala G., (2015) Predictions of corrosion current density and potential by using chemical composition and corrosion cell characteristics in microalloyed pipeline steels, Measurment, 62, 97-107.
21. Faizabadi M. J. , Khalaj G. , Pouraliakbar H. and Jandaghi M. R. , (2014) Predictions of toughness and hardness by using chemical composition and tensile properties in microalloyed line pipe steels, Neural Computing and Applications, 25, 1993–1999.
22. Fouda1 Abd El-Aziz S., Abd El-Maksoud, Samar A., Abd El-Salam Samar A., (2017) Mitigation of corrosion of carbon steel in acid medium using some antipyrine derivatives, Zastita Materijala, , 58 (1), 5 – 15
23. Narayan R., (1983) An Introduction to Metallic Corrosion and its Prevention, Oxford, New Delhi, p73.
24. Ailor W. H., (1971) "Handbook of Corrosion Testing and Evaluation", John Wiley &Sons, Inc., New York, 173-174.
25. Dacres Sutula C. M., A Larrick B. F., (1983) Comparison of Procedures Used in Assessing the Anodic Corrosion of Metal Matrix Composites and Lead Alloys for Use in Lead‐Acid Batteries, Electrochem. Soc., 130, 981-985.
26. Crow D. R., (1988) Principles and Applications of Electrochemistry, Chpman and Hall, London, 3rd ed..
27. Moretti G., Quartanone G., Tassan A., Zingales A., (1994) Inhibition of mild steel corrosion in 1N sulphuric acid through indole ,Wekst. Korros., 45, 641-647.
28. Pourbaix M., (1966)"Atlas of Electrochemical Equilibria, In Aqueous Solutions", Pergamon Press, Oxford.
29. Fouda A. S., El- Defrawy A. M., El-Sherbeni M. W., (2012) Pharmaceutical compounds as save corrosion inhibitors for CS in 1 M H_2SO_4 solution, J. Chem., 39, 1-27.
30. Ali Adel H., (2018) Electrochemical study for Effect of Gliclazide as a Corrosion Inhibitor of the Carbon Steel in Sulfuric Acid Medium by Applied Potentiodynamic and Evans Techniques, International Journal of Modern Chemistry, 10 (2), 233-255.

31. Ali Adel H., (2020) Electrochemical Behavior of Quench-treated Low Carbon Steel in 0.5 H2SO4 Medium Containing Simvastatin Drug as Corrosion Inhibitor Using Potentiodynamic and Evans Techniques, International Journal of Modern Chemistry, 12(1), 117-140.
32. Fouda A. S., El-Ewady G., Ali Adel H., (2017) Corrosion Inhibition of Carbon Steel in hydrochloric acid medium using gliclazide drug, Journal for Electrochemistry and Plating Technology, November, , 1-20.
33. Fouda A.S., El-Ewady G., Ali A.H., (2017) Modazar as promising corrosion inhibitor of carbon steel in hydrochloric acid solution, Green Chem. Lett. Rev., 10 (2), 88–100.
34. Fouda A.S., El-Ewady G., Ali Adel H., (2017) Corrosion protection of carbon steel by using simvastatin drug in HCl medium, J. Applicable Chem., 6 (5), 701-718.
35. Abd El-Aziz, S. Fouda, Adel H. Ali, (2018) Egy-dronate drug as promising corrosion inhibitor of C-steel in aqueous medium, Jour. Mater. Prot., 59, 126-140.
36. Ali Adel H., (2018) Electrochemical study of candesartan drug as corrosion inhibitor for carbon steel in acid medium, J. Adv. Electrochem., 4 (1), 152–157.
37. Jan Mohammad Mir, R.C. Maurya, P.K. Vishwakarma, (2017) Corrosion resistance and thermal behavior of acetylacetonato-oxo peroxo molybdenum (VI) complex of maltol: Experimental and DFT studies, Karbala International Journal of Modern Science, 3, 212-223
38. Fouda Abd El-Aziz S., El-Hossiany Ahmed A., Ramadan Heba M., (2017) Calotropis procera plant extract as green corrosion inhibitor for 304 stainless steel in hydrochloric acid solution, Zastita Materijala 58 (4), 541 - 555
39. Ali Adel H., Fouda Abd El-Aziz S., Tilp Amal H., (2020) Electrochemical behavior for corrosion protection of mild steel (MS) in 1M HCl medium by using lidocaine drug as an inhibitor, Zastita Materijala 61 (4), 286 - 305
40. Ali Adel H., (2020) Electrochemical Behavior of Quenching Low Carbon Steel (LCH) by using Simvastatin Drug as a Corrosion Protection in 0.5 H_2SO_4 Medium by Applied: Potentiodynamic and Evans Techniques, Global Journal of Science Frontier Research: B Chemistry, 20 (2), 23-39

London Journal Press Membership

For Authors, subscribers, Boards and organizations

London Journals Press membership is an elite community of scholars, researchers, scientists, professionals and institutions associated with all the major disciplines. London Journals Press memberships are for individuals, research institutions, and universities. Authors, subscribers, Editorial Board members, Advisory Board members, and organizations are all part of member network.

Read more and apply for membership here:
https://journalspress.com/journals/membership

For Authors

Author Membership provide access to scientific innovation, next generation tools, access to conferences/seminars /symposiums/webinars, networking opportunities, and privileged benefits.
Authors may submit research manuscript or paper without being an existing member of LJP. Once a non-member author submits a research paper he/she becomes a part of "Provisional Author Membership".

For Institutions

Society flourish when two institutions come together." Organizations, research institutes, and universities can join LJP Subscription membership or privileged "Fellow Membership" membership facilitating researchers to publish their work with us, become peer reviewers and join us on Advisory Board.

For Subscribers

Subscribe to distinguished STM (scientific, technical, and medical) publisher. Subscription membership is available for individuals universities and institutions (print & online). Subscribers can access journals from our libraries, published in different formats like Printed Hardcopy, Interactive PDFs, EPUBs, eBooks, indexable documents and the author managed dynamic live web page articles, LaTeX, PDFs etc.

GO GREEN AND HELP
SAVE THE ENVIRONMENT

JOURNAL AVAILABLE IN

PRINTED VERSION, INTERACTIVE PDFS, EPUBS, EBOOKS, INDEXABLE DOCUMENTS AND THE AUTHOR MANAGED DYNAMIC LIVE WEB PAGE ARTICLES, LATEX, PDFS, RESTRUCTURED TEXT, TEXTILE, HTML, DOCBOOK, MEDIAWIKI MARKUP, TWIKI MARKUP, OPML, EMACS ORG-MODE & OTHER

SCAN TO KNOW MORE

support@journalspress.com
www.journalspress.com

*THIS JOURNAL SUPPORT AUGMENTED REALITY APPS AND SOFTWARES